CrossMark

ORIGINAL PAPER

Geochemistry and mineralogy of the Al-rich shale from Baluti formation, Iraqi Kurdistan region: implications for weathering and provenance

Faraj H. Tobia[1] · Baran H. Mustafa[1]

Abstract The mineralogical and geochemical characteristics of the Upper Triassic Baluti shale from the Northern Thrust Zone (Sararu section) and High Folded Zone (Sarki section) Kurdistan Region, Iraq, have been investigated to constrain their paleoweathering, provenance, tectonic setting, and depositional redox conditions. The clay mineral assemblages are dominated by kaolinite, illite, mixed layers illite/smectite at Sararu section, and illite > smectite with traces of kaolinite at Sarki. Illite, to be noted, is within the zone of diagenesis. The non-clay minerals are dominated by calcite with minor amounts of quartz and muscovite in Sararu shale; and are dominated by dolomite with amounts of calcite and quartz in Sarki shale. Baluti shale is classified as Al-rich based on major and minor elements. The chemical index of alteration (CIA) is significantly higher in the Sararu than the Sarki shales, suggesting more intense weathering of the Sararu than the Sarki shales. The index of compositional variability (ICV) of the Sararu shale is less than 1 (suggesting it is compositionally mature and was deposited in a tectonically quiescent setting). More than 1 for Sarki shales (suggest it is less mature and deposited in a tectonically active setting). Most shale of the Baluti plot parallel and along the A-K line in A-CN-K plots suggest intense chemical weathering (high CIA) without any clear-cut evidence of K-metasomatism. Clay mineral data, Al enrichment, CIA values, and A-CN-K plot suggest that the source area experienced high degree of chemical weathering under warm and humid conditions, especially in Sararu. Elemental ratios critical of provenance (La/Sc, Th/Sc, Th/Cr, Th/Co, Ce/Ce*$_{PN}$, Eu/Eu*$_{PN}$, and Eu/Eu*$_{CN}$) shows slight difference between the Sararu and Sarki shales; and the ratios are similar to fine fractions derived from the weathering of mostly felsic rocks. The Eu/Eu*$_{CN}$, Th/Sc, and low K_2O/Al_2O_3 ratios of most shales suggest weathering from mostly a granodiorite source rather than a granite source, consistent with a source from old upper continental crust. Discrimination diagrams based on major and trace element content point to a role of the felsic-intermediate sources for the deposition of Baluti Formation, and probably mixed with mafic source rocks at Sararu section. The chondrite-normalized rare earth elements (REE) patterns are similar to those of PAAS, with light REE enrichment, a negative Eu anomaly, and almost flat heavy REE pattern similar to those of a source rock with felsic components. The source of sediments for the Baluti Formation was likely the Rutba Uplift and/or the plutonic-metamorphic complexes of the Arabian Shield located to the southwest of the basin; whereas the Sararu shale was affected by the mafic rocks of the Bitlis-Avroman-Bisitoun Ridge to the northeast of Arabian Plate. The tectonic discrimination diagrams, as well as critical trace and REE characteristic parameters imply rift and active setting for the depositional basin of the shale of Baluti Formation. The geochemical parameters such as U/Th, V/Cr, V/Sc, and Cu/Zn ratios indicate that these shales were deposited under oxic environment and also show that Sarki shale was deposited under more oxic environment than Sararu.

✉ Faraj H. Tobia
faraj.tobia@su.edu.krd

1 Department of Geology, Salahaddin University, Kurdistan Region, Iraq

🖄 Springer

Introduction

The mineralogy and geochemistry of siliciclastic sediments have been widely used to determine the degree of weathering (Nesbitt and Young 1982; Fedo et al. 1995; Nyakairu and Koeberl 2001; Ghandour et al. 2003; Hosseininejad et al. 2012; Srivastava et al. 2013; Akinyemi et al. 2013; Zhang et al. 2013), source rock composition (Tawfik et al. 2011; Cao et al. 2012; Armstrong-Altrin et al. 2012, 2014; Dai et al. 2016), tectonic setting (Dickinson and Suczek 1979; Bhatia 1983; Verma and Armstrong-Altrin 2013), and diagenesis (Zaid 2015; Zaid and Gahtani 2015; Zaid et al. 2015), as well as paleogeographic reconstruction of provenance (Zimmermann and Spalletti 2009; Armstrong-Altrin 2015).

The shale-dominated Baluti Formation (Upper Triassic strata) is distributed in the Northern Thrust Zone and High Folded Zone in North Iraq (Fig. 1a). The Baluti Formation consists mainly of shale with intercalations of thin bedded dolomitized limestones. It varies in thickness from 35 to 60 m in surface sections; but it varies between 25 and 80 m in the subsurface sections (Buday 1980). However, fossils are rare and not age diagnostic (Bellen et al. 1959). Therefore, the age of the formation is arbitrary and determined by its stratigraphic position between the proved Upper Triassic (Norian) Kurra Chine Formation and the overlying Sarki Formation (Liassic) (Fig. 2). However, Hanna (2007) suggested the formation age to be Carnian based on the assemblage palynozones; whereas, equivalent formations in west Iraq may be eroded (Jassim et al. 2006).

The Baluti Formation has not been fully studied by geologist, except for a few ones which included general description (Bolton 1958; Bellen et al. 1959) and age determination (Hanna 2007). Moreover, there are no previous studies available on the mineralogy and geochemistry. Similarly, there are no studies that focused on provenance, tectonic setting, and paleoweathering of the Baluti Formation. In this paper, therefore, the authors examine the mineralogy and geochemistry of the Al-rich shale of the Baluti Formation through two sections in the Sararu section in the Northern Thrust Zone and Sarki section in the High Folded Zone. The aim of this study is to identify the source rock characteristics and the paleoweathering as well as the paleo-oxygenation conditions of the Upper Triassic in the northeast margin of the Arabian Plate.

Geological background

The Baluti Formation belongs to tectonostratigraphic megasequence AP6, which the latter started from Mid-Permian to Early Jurassic (255–182 Ma). During Late Permian time, the Neo-Tethys Ocean opened when one or more narrow blocks of continental crust drifted away from the NE margin of Gondwana. This megasequence (AP6) was deposited on the north and east facing passive margin of the Arabian Plate. The unconformity at the base of the megasequence was a break up unconformity (Jassim and Goff 2006).

Renewed rifting occurred within this passive margin in Mid-Late Triassic time (Fig. 1b) creating a broad and highly restricted intra-shelf basin in Mesopotamia separated from the open ocean by a narrow rift with alkali basalts and an outer ridge of thinned continental crust on which an open marine carbonate platform developed (Numan 1997; Jassim and Goff 2006). This phase of rifting was followed by slow thermal subsidence in Norian-Liassic time and led to the formation of a passive margin megasequence along northern and eastern margins of the Arabian plate, and the development of the Mesopotamian basin. The Rutba Uplift developed in the area now representing west Iraq, northeast Jordan, east Syria, and northwest Saudi Arabia (Fig. 1). The Upper Permian and Lower Triassic sediments were deposited on a broad platform (Jassim and Goff 2006).

The Arabian Shield (the southwestern part of Arabian Plate) is composed of accreted Neoproterozoic juvenile volcanic arcs, gneisses, metagabbros, metavolcano-sedimentary sequences, granites, and gabbro-diorite complexes (Stern 1994). At about 580–540 Ma, the Arabian Shield crust stabilized, accompanied by continental-scale uplift, erosion, and the development of intra-mountain basins and rifting (Moghazi 2003; Avigad et al. 2005).

The lower contact with the underlying Norian Kurra Chine Formation comprises of monotonous dark brown and black limestone ranging in thin and thick-bedded, with occasional beds of thick bedded fetid dolomite with slump structures, and papery shale. The upper boundary of Baluti Formation is conformable with the Liassic Sarki Formation, which is composed of about 300 m of carbonate rocks. The Baluti Formation attains a thickness of 66 m and consists of gray shale with thin bedded carbonate rocks at Sararu section, and 43 m of gray to grayish black shale interbedded with thin layer of carbonate rocks at Sarki section. Hanna (2007) estimated the age of the formation by assemblage palynozones that the upper part of Baluti Formation is of Carnian (Julian) age. He suggested the prevalence of shore zone depositional environment with influence of fresh water for the lower portion of the upper part of the formation. He proposed the influence of open marine conditions on the deposition of the upper portion of the formation.

Sampling and methods

Twenty-seven fresh shale samples were collected from two outcrop sections (Sararu section = 15 samples and Sarki section = 12 samples) of Baluti Formation for
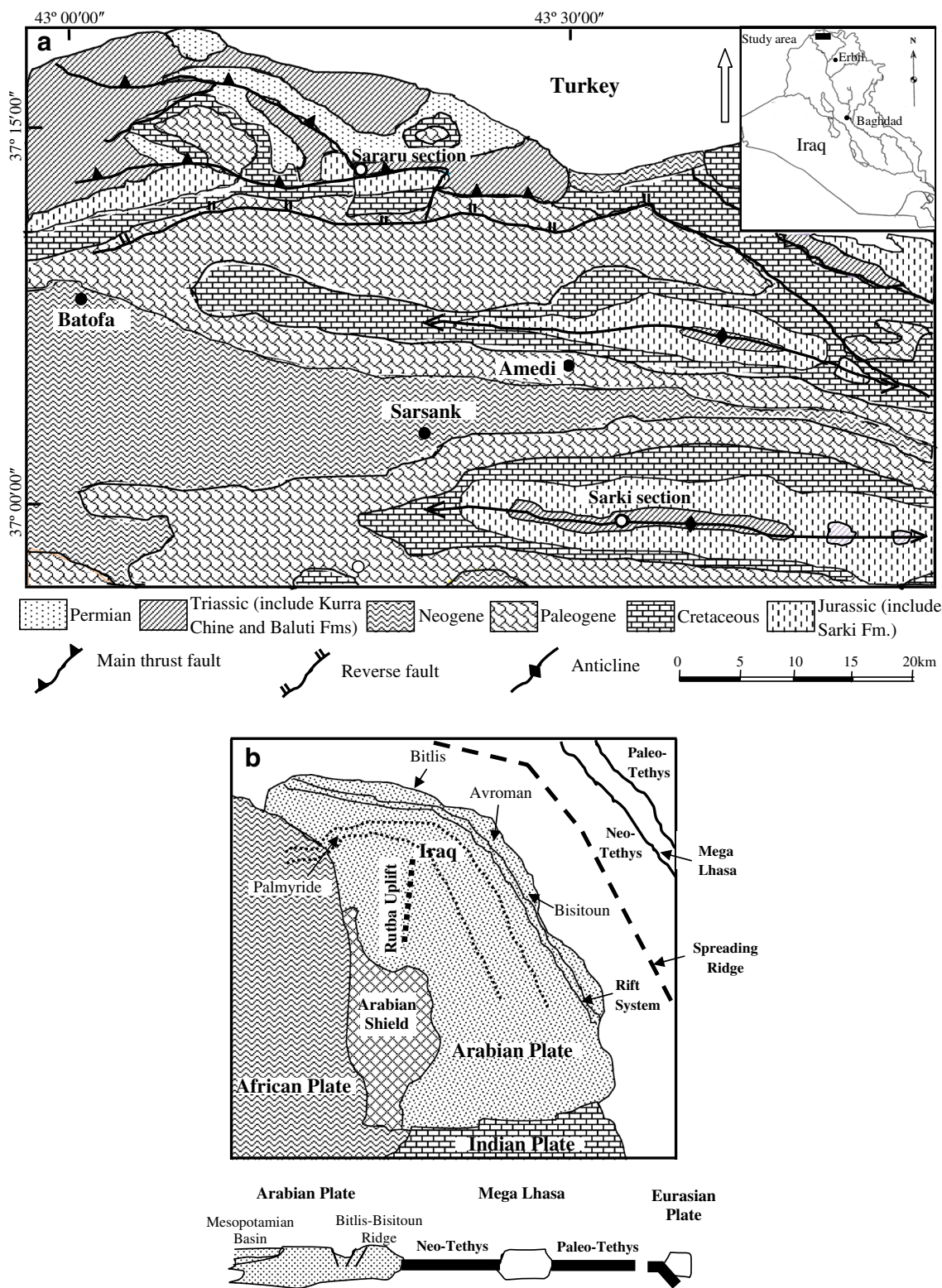
Fig. 1 **a** Geological map and the location of the studied sections, (enlarged from Sissakian 2000). **b** Mid Triassic-Norian geodynamic development of the Arabian Plate (Jassim and Goff 2006)

whole-rock geochemical analyses. The studied samples are collected from two outcrop sections: The first locality lies at Sararu Village which is located at about 26 km

northwest of Amedi Town, at latitude 37° 14′ 21″ N and longitude 43° 16′ 56″ E in the Northern Thrust Zone. The second locality is about 15 km southeast of Amedi Town,

Fig. 2 Columnar sections of Baluti Formation: **a** Sararu and **b** Sarki sections

Sample	Lithology	Lithologic description
		Carbonate rocks of Sarki Fm.
★		Grey calcareous shale
★		Dark grey marl with thin layer of hard limestone
★		Grey calcareous shale with thin layer of argillaceous limestone
★		Grey calcareous shale with thin layers of hard limestone
★		Grey calcareous shale with thin layer of hard limestone
		Calcareous shale interbedded hard limestone
★		Grey calcareous shale with thin layers of hard and fractured limestone
★		Grey calcareous shale with thin layer of hard limestone
★		Dark grey shale and limestone
★		Grey cal. shale with limestone
		Grey limestone
★		Cal. shale with hard limestone
★		Dark limestone with calc. shale
★★		Limestone with calc. shale
		Carbonate rocks of Kurra Chine Fm.

a   **Sararu section**   Scale 1:800

Sample	Lithology	Lithologic description
		Carbonate rocks of Sarki Fm.
★		Dark grey shale with limestone
★		Greyish black shale interbedded with thin beds of limestone
		Dark grey limestone
★		Greyish black shale
★		Greyish black shale interbedded with thin beds of limestone
★		Yellowish grey calcareous shale
		Brecciated limestone
★		Greyish black shale interbedded with thin layers of limestone
★		Greyish black shale
★		Bedded limestone with yellowish black shale
★		Yellowish green shale
★		Greenish shale with limestone
★		Yellowish grey calcareous shale
		Carbonate rocks of Kurra Chine Fm.

b   **Sarki section**   Scale 1: 500

▨ Limestone   ▨ Calcareous shale   ▨ Marl   ▨ Shale   ★ Sample location

in the core of Gara anticline near Sarki Village which is situated at latitude 36° 59′ 34″ N and longitude 43° 32′ 23″ E in High Folded Zone (Fig. 1). Details of sample locations and lithology are presented in Fig. 2. Samples for geochemical analysis were first crushed and then powdered to 200 mesh with an agate pulverizer. The mineralogy of 15 shale samples (8 from Sararu and 7 from Sarki shales) was determined by conventional x-ray diffraction (XRD) method using Philips PM8203 x-ray diffractometer with Ni-filtered CuKα radiation using 40 kV–40 mA at the x-ray laboratories of the Iraqi Geological Survey, Baghdad, Iraq. The samples were analyzed using a scan range from 3° to 50° 2θ for the crushed bulk samples and from 3° to 20° 2θ for the clay fraction at an interval of 0.02° 2θ per second using a rotating sample holder. The clay sized fraction (<2 μm) was separated out from the shale by disaggregating and dispersing the sample in distilled water by pipette method, and oriented slides were prepared to obtain a good reflection (Friedman and Johnson 1982; Hardy and Tucker 1988). The oriented mounts were run under three separate conditions: air-dry state, after ethylene glycol treatment at 25 °C for 15 h, and after heating to 550 °C for 1 h for discrimination between kaolinite and chlorite. For the semi-quantification of the identified principal minerals, peak

areas of the specific reflections of the main clay minerals were calculated (Grim 1968; Carroll 1970).

The twenty-seven samples were analyzed for major oxides (TiO_2, Al_2O_3, Fe_2O_3, MnO, MgO, CaO, Na_2O, K_2O, and P_2O_5) and SO_3 by x-ray fluorescence (XRF); trace elements (Sc, V, Cr, Co, Ni, Cu, Zn, Rb, Sr, Y, Zr, Nb, Mo, Ba, Hf, Th, and U); and rare earth elements (REEs) (La, Ce, Pr, Nd, Sm, Eu, Gd, Tb, Dy, Er, Ho, Tm, Yb, and Lu) were analyzed by inductively coupled plasma-mass spectrometry (ICP-MS) in the ALS international laboratory in Spain. Loss on ignition (LOI) data was determined from the total weight after drying the samples in oven 100 °C for 24 h, to remove moisture content, next ignition the samples at 1000 °C for 2 h in the Department of Geology laboratory (Salahaddin University, Kurdistan Region, Iraq). SiO_2 was calculated after subtracting the summation of major elements and LOI from 100.

Chemical analysis for major elements has precisions up to 3 %; whereas it varies between 1 and 8 % for the trace and REEs. Internationally recognized standard materials GBM908-5 and OGGeo08 were used as references. Based on these standards, the accuracy and precision of the analysis were within ±2 % for elements Nb, Sr, Sc, Th, U, V, Zr, Cu, Pb, Zn, Mo, Ni, Pr, Nd,

Sm, Ho, and Tm; ±5 % for Ba, Hf, Rb, Y, La, Ce, Eu, Tb, Dy, Er, and Lu; and ±10 % for Gd and Yb.

Comparison of data between the present study and the published data of Post Archean Australian Shale (PAAS) was done whenever possible. The REE data were normalized to the chondrite values of Taylor and McLennan (1985). The normalized Eu anomaly $(Eu/Eu^*)_{CN}$ is also a useful discriminator between samples and between plate tectonic settings (McLennan 1989; $Eu/Eu^* = Eu_{CN}/(Sm_{CN} \times Gd_{CN})^{1/2}$, where the subscript $_{CN}$ denotes chondrite normalized values). The normalized REE data to PAAS are a useful discriminator for the source rock (Dai et al. 2016; $Ce/Ce^* = Ce_{PN}/(0.5 \, Ln_{PN} + 0.5 \, Pr_{PN})$ and $Eu/Eu^* = Eu_{PN}/(0.5 \, Sm_{PN} + 0.5 \, Nd_{PN})$ where the subscript $_{PN}$ denotes PAAS normalized values.

The chemical index of alteration (CIA), plagioclase index of alteration (PIA), and index of compositional variation (ICV) were calculated following the methods of Nesbitt and Young (1982), Fedo et al. (1995) and Cox et al. (1995), respectively. CaO was corrected by the methodology proposed by McLennan et al. (1993), in which CaO values were accepted only if CaO < Na_2O; when CaO > Na_2O, it was assumed that the concentration of CaO equals Na_2O.

Results

Mineralogy

Mineral compositions from XRD analyses are listed in Table 1 and representative XRD diagrams are shown in Fig. 3. The Sararu and Sarki samples show a contrasting mineralogy. The Sararu samples are mainly composed of clay minerals associated with calcite, quartz, and small amounts of muscovite; and the principal clay minerals are illite, kaolinite, and mixed layer illite/smectite. However, the Sarki samples are composed of clay minerals associated with dolomite, quartz, and calcite; and the clay minerals are illite, smectite, with trace amounts of kaolinite. Calcite and quartz represent 92.67 and 6.40 %, respectively, of the non-clay minerals in Sararu shale while dolomite, quartz, and calcite represent 50.46, 32.25, and 15.92 %, respectively, in Sarki shale (Table 1). Marine shales contain relatively higher calcite content than non-marine shales. However, calcite varies from 22 to 80 vol % in marine shales with values less than 4 vol % are detected in non-marine shales (Ghandour et al. 2003).

The clay minerals identified in the <2-μm fractions are illite, kaolinite, and mixed layer illite/smectite. Illite and kaolinite are generally the dominant clay minerals in the Sararu samples and their proportions range from 27.00 to 57.60 and from 6.90 to 54.40 %, respectively.

Illite and smectite are the dominant clay minerals in the Sarki samples and their proportion range from 63.20 to 72.70 and from 20.90 to 36.80 %, respectively. The Kübler Index (KI) values for the samples range between 0.80 and 1.20 $\Delta 2\theta$ (average = 1.0 $\Delta 2\theta$) in Sararu and from 0.70 to 1.00 $\Delta 2\theta$ (average = 0.83 $\Delta 2\theta$) in Sarki section (Table 1); the modal illite crystallinity value is 0.69 $\Delta 2\theta$, typical values of a high diagenetic zone (Merriman and Frey 1999). The average of illite chemistry and kaolinite crystallinity indices are 0.59 and 0.15 for Sararu and are 0.55 and 0.23 for Sarki.

Geochemistry

The major, trace, and rare earth elements analysis results of the Al-rich shale from Baluti Formation are presented in Tables 2 and 3.

Major elements

The Upper Triassic shale rocks show significant mineralogical variability, which is reflected in the variation of the chemical composition (Table 1). The shale of the Baluti Formation has high CaO content in Sararu section (17.36–38.92 %, average 33.09 %) and 4.12–35.84 %, average 14.00 % in Sarki section. The higher content of CaO has a great dilution effect on other oxides. The SiO_2 content in the Sararu section ranges between 4.86 and 18.38 % with an average of 9.12 %; and it varies in the Sarki section from 11.72 to 27.64 % with an average of 19.06 %. Al_2O_3 ranges from 9.95 to 23.94 % with an average of 14.60 % in the Sararu section; whereas it varies in the Sarki section between 12.03 and 30.91 % with an average of 19.43 %. The TiO_2 content of both sections is relatively low; it ranges between 0.30 and 0.79 % with an average of 0.48 % in Sararu; and ranges between 0.25 and 0.78 % with an average of 0.49 % in the Sarki section. The content of Fe_2O_3 in the shale of the Sararu section ranges between 4.29 and 7.12 % with an average of 5.64 %; on the other hand, it ranges between 5.69 and 11.73 % with an average of 8.23 % in the Sarki section. The enrichment of CaO as well as the significant correlation between CaO and LOI ($r = 0.780$, $n = 12$) in the Sarki section (Table 4) suggest that LOI and CaO are incorporated into calcite rather than plagioclase. Al_2O_3 and K_2O content can be related to the presence of mica and clay minerals ($r = 0.916$, $n = 12$) and Al distribution that is controlled by the content of clay minerals (McLennan et al. 1983). The Na_2O content is principally related to clay minerals and it significantly correlates with K_2O ($r = 0.886$ and 0.753, $n = 15$ and 12 for Sararu and Sarki, respectively) as shown in Table 4. Higher Fe_2O_3 could be related to the presence

Table 1   Semi-quantitative mineralogical composition and crystallographic parameters of the shale from the Baluti Formation

| Sample no.	Non-clay minerals 100 %				Clay minerals 100 %						
	Calcite %	Dolomite %	Quartz %	Muscovite %	Kaolinite %	Illite %	Smectite %	Illite-smectite %	Illite crystallinity index	Illite chemistry index	Kaolinite crystallinity index
Sararu section											
BS.1	91.45	–	7.43	1.12	10.70	51.80	–	37.50	0.80	0.88	0.15
BS.3	89.30	–	10.70	–	46.00	27.00	–	27.00	1.20	0.58	0.05
BS.5	95.10	–	4.90	–	41.80	30.70	–	27.50	1.00	0.85	0.05
BS.7	95.10	–	4.90	–	44.50	29.40	–	26.10	1.20	0.58	0.04
BS.9	94.25	–	4.89	0.86	38.80	30.60	–	30.60	0.80	0.13	0.03
BS.11	91.92	–	6.73	1.35	54.40	30.80	–	14.80	1.00	0.51	0.05
BS.13	91.27	–	6.72	2.01	6.90	57.60	–	35.50	1.20	0.72	0.72
BS.15	92.96	–	5.63	1.41	14.90	35.90	–	49.20	0.80	0.45	0.13
Average	92.67		6.40	0.84	32.30	36.7 0		31.00	1.00	0.59	0.15
Sarki section											
B.1	63.45	27.74	8.81	–	3.10	68.40	28.50	–	0.75	0.45	0.32
B.3	13.14	9.54	77.32	–	6.30	67.60	26.10	–	1.00	0.70	0.19
B.5	11.06	55.89	33.05	–	6.90	65.40	27.70	–	0.70	0.44	0.42
B.7	–	84.09	15.91	–	5.40	67.80	26.80	–	0.95	0.53	0.20
B.8	9.84	64.18	25.98	–	6.70	71.10	23.20	–	0.90	0.68	0.18
B.10	7.24	41.21	42	9.55	6.40	72.70	20.90	–	0.83	0.38	0.32
B.12	6.70	70.59	22.71	–	–	63.20	36.80	–	0.70	0.71	–
Average	15.92	50.46	32.25	1.36	4.97	68.00	27.00	–	0.83	0.55	0.23

of iron oxide, heavy minerals, or hematite cement. MgO is significantly correlated with CaO ($r = -0.754$, $n = 15$) in the Sararu section. CaO content is mostly related to the presence of calcite cements or skeletal fragments (Khanehbad et al. 2012). Significant correlation between Al_2O_3 and Fe_2O_3 in the Sarki shale (Table 4) implies that Fe is partly controlled by clay minerals. The high K_2O/Na_2O ratios (35.89 and 41.06 for Sararu and Sarki, respectively) are due to the presence of K-bearing minerals such as mica and illite (Khanehbad et al. 2012). In these samples, TiO_2 has a positive correlation with Al_2O_3 ($r = 0.772$ and 0.930, $r = 12$ and 15 for Sararu and Sarki, respectively), which suggests that TiO_2 is possibly associated with phyllosilicate minerals (Dabard 1990) or may largely occur in kaolinite because Ti can substitute Al (Dai et al. 2015). It also indicates chemical weathering in the source area that caused the concentration of these residual elements (Dokuzi and Tanyolu 2006). The ternary diagram based on major and minor elements (Al_2O_3, TiO_2, and Zr), that are usually considered the least mobile during chemical weathering was first suggested by Garcia et al. (1994). In this study, all the samples fall in the line of Al-rich shales and are classified as Al-rich shale (Fig. 4).

Trace elements

Large ion lithophile elements (Rb, Ba, and Sr)

In comparison with PAAS (Table 2), the Upper Triassic samples generally tend to display more depleted large ion lithophile element (LILE) patterns. The mean LILE concentrations of the shale are slightly to moderately depleted; whereas the mean Sr concentrations are moderately enriched (especially in the Sararu section). The Sr enrichments are in accordance with high carbonate (calcite in Sararu and dolomite in Sarki). The Rb and Ba have significant positive correlation coefficients with Al_2O_3 in Sarki (0.944 and 0.967, respectively; $n = 12$) and weak in Sararu (0.462 and 0.483, respectively; $n = 15$). The correlation coefficients of K_2O with Rb in Sarki is 0.882 and with Ba is 0.938 ($n = 12$) and in Sararu is 0.894 with Rb and is 0.661 ($n = 15$) with Ba, as shown in Table 4. These correlations suggest that their distributions are controlled by kaolinitic, smecitic, and illitic phyllosilicate phases. No positive correlations have been found between Sr and other oxides, except with CaO (0.820 in Sararu and 0.793 in Sarki); this indicates the association of Sr in the carbonate phase (Yan et al. 2007).

Fig. 3 X-ray diffractograms of selected shale samples from Sararu and Sarki sections, Baluti Formation
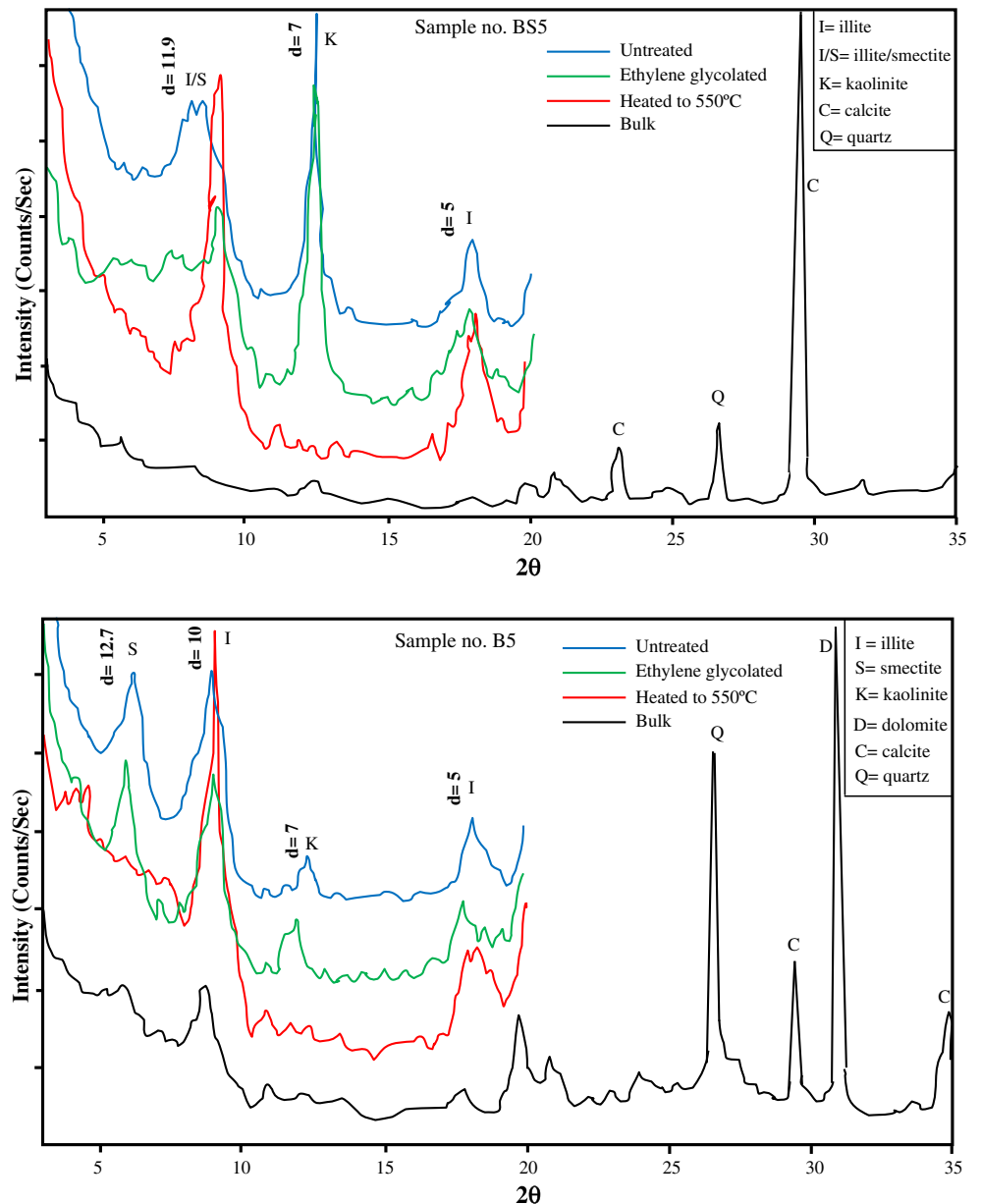
High-field strength elements (Th, U, Y, Zr, Nb, and Hf)

The Baluti shales, compared with the PAAS, are characterized by depletion of high-field strength elements (HFSE) except Nb (in Sarki). High-field-strength element concentrations show significant positive correlations with SiO_2, Al_2O_3, Na_2O, K_2O, and TiO_2 (except U with Na_2O and K_2O in the Sararu section; as displayed in Table 4); this indicates their clay mineral control. The average Th/U ratio in Sararu (2.09) is lower than in the Sarki shale (2.82) and both are lower than PAAS (4.7; Taylor and McLennan 1985). The Th/Sc ratio, a good indicator of provenance, has average

values of 0.77 and 0.61 for the Sararu and Sarki shales, respectively. Furthermore, strong positive correlation between Zr and Hf as attested by their high correlation coefficients (0.957 and 0.991 as in Table 4), indicates they are similar during magmatic differentiation (Dokuzi and Tanyolu 2006). Both shales in Sararu and Sarki show strong positive correlation between Zr and TiO_2 (r = 0.771 and 0.936, respectively); this suggests the concentration of certain accessory minerals such as zircon, monazite, ilmenite, and rutile. Y has strong positive correlation with REE (particularly with Ho and Dy) in Sararu and Sarki (0.986 and 0.863, respectively) due to the similar geochemical affinities. The significant

Table 2 Major (%) and trace (ppm) element concentrations and elemental ratios for Al-rich shale of the Baluti Formation, and for Post-Archean Australian average shale (PAAS)

Sample no.	Sararu section															average
	BS.1	BS.2	BS.3	BS.4	BS.5	BS.6	BS.7	BS.8	BS.9	BS.10	BS.11	BS.12	BS.13	BS.14	BS.15	
SiO_2	10.4	8.48	18.4	10.3	6.45	11.4	6.48	11.2	8.06	4.86	9.33	5.14	8.55	5.95	11.6	9.12
TiO_2	0.43	0.46	0.72	0.59	0.4	0.79	0.46	0.36	0.38	0.37	0.56	0.47	0.5	0.3	0.47	0.48
Al_2O_3	12.8	14.2	12.8	18.0	12.0	24.0	14.8	14.0	12.0	11.2	18.0	14.9	15.8	9.95	14.7	14.6
Fe_2O_3	4.29	4.86	6.98	6.35	6.44	5.98	5.18	5.49	5.38	7.12	5.29	4.92	5.12	5.58	5.69	5.64
MnO	0.01	0.01	0.02	0.02	0.02	0.02	0.02	0.04	0.02	0.02	0.02	0.02	0.02	0.01	0.01	0.02
MgO	0.96	0.86	0.66	0.65	1.29	0.81	0.6	12.3	0.63	0.70	0.5	0.68	0.76	1.08	0.75	1.55
CaO	35.7	35.4	28.8	31.1	36.7	26.0	36.4	17.4	37.0	38.4	32.1	36.7	33.6	38.9	32.3	33.1
Na_2O	0.08	0.08	0.11	0.08	0.08	0.11	0.08	0.16	0.08	0.08	0.08	0.08	0.08	0.08	0.08	0.09
K_2O	3.23	2.94	3.78	2.89	2.22	3.74	2.63	6.1	2.27	2.77	2.75	3.42	3.93	2.6	3.11	3.23
P_2O_5	0.18	0.18	0.21	0.21	0.22	0.18	0.21	0.15	0.22	0.22	0.22	0.26	0.23	0.22	0.23	0.21
SO_3	0.13	0.13	0.08	0.08	0.63	0.08	0.18	0.13	0.38	1.1	0.25	1.2	0.05	2.1	0.1	0.44
LOI	31.8	32	27.4	29.8	33.6	27	33	32.8	33.6	33.2	31	32.2	31.4	33.2	31	31.53
Sc	7.5	8.1	11.8	10.1	6.9	12.7	7.4	6.9	6.3	6.1	8.6	7.3	8.4	5.4	7.5	8.1
V	100	112	175	150	98	182	115	48	111	99	149	123	139	91	123	121
Cr	54	51	70	59	78	99	57	32	50	51	63	53	56	44	55	58.1
Co	6.3	7.2	9.5	8.3	6.4	13.6	6.4	5.8	5.3	5.1	7.3	6.5	10.0	4.5	5.8	7.2
Ni	39.5	41.5	58.3	52.8	43	67.6	48.2	17.6	42.1	39	42	50.6	52.8	41.3	46.2	45.5
Cu	9.3	10.5	15.4	13.4	34.4	38.3	12.7	15.2	12.5	15.1	11.3	13.8	15.0	13.2	11.4	16.1
Zn	48	15	78	89	66	108	45	24	15	12	44	16	58	81	56	50.3
Rb	33.7	35.3	47.1	36.3	28.2	52.1	33.3	64.5	27.6	25.3	33.4	33.2	36.7	25.4	32.7	36.3
Sr	497	449	495	527	696	409	653	110	611	516	404	545	360	604	475	490
Y	14.9	15.9	20.9	18.9	15.4	21	14.7	13.9	12.5	12.3	15.4	14.1	16.7	11.6	13.9	15.4
Zr	74.2	76.7	149	102	65.7	133	71.1	121.5	63.7	62.1	85	69.4	86.5	54.8	72.4	85.8
Nb	10.7	11.4	17.8	14.3	9.9	19.7	11.5	19.8	9.3	8.4	12.9	11.1	12.3	7.3	11.2	12.5
Mo	2.6	2.7	4.7	5.6	5.3	5.5	5.0	1.6	5.1	3.5	6.0	7.8	17.6	4.6	9.1	5.8
Ba	40	50	60	50	40	60	40	60	30	30	40	40	40	40	40	44
Hf	2.1	2.1	3.2	2.7	1.8	3.5	2	2.9	1.7	1.7	2.4	2.1	2.3	1.3	2.1	2.2
Th	5.7	6.2	9	7.8	5.2	9.5	5.8	4.4	5	4.8	6.9	5.8	6.7	4.4	6.1	6.2
U	2.3	3.1	3	3.1	2.6	3.4	2.7	3.6	2.8	2.6	2.9	3	3.4	2.8	3.5	2.9
SiO_2/Al_2O_3	0.81	0.6	1.43	0.57	0.54	0.48	0.44	0.8	0.67	0.43	0.52	0.34	0.54	0.6	0.79	0.62
Al_2O_3/TiO_2	29.8	30.9	17.8	30.5	30.0	30.3	32.1	38.9	31.7	30.3	32.1	31.8	31.5	33.2	31.2	30.4
K_2O/Na_2O	40.4	36.8	34.4	36.1	27.8	34.0	32.9	38.1	28.4	34.6	34.4	42.8	49.1	32.5	38.9	35.9
K_2O/Al_2O_3	0.25	0.21	0.29	0.16	0.19	0.16	0.18	0.44	0.19	0.25	0.15	0.23	0.25	0.26	0.21	0.22
Fe_2O_3/TiO_2	9.98	10.6	9.69	10.8	16.1	7.57	11.3	15.3	14.2	19.2	9.5	10.5	10.2	18.6	12.1	11.8
Th/Sc	0.76	0.77	0.76	0.77	0.75	0.75	0.78	0.64	0.79	0.79	0.8	0.79	0.8	0.81	0.81	0.77
Zr/Sc	9.89	9.47	12.6	10.1	9.52	10.5	9.61	17.6	10.1	10.2	9.88	9.51	10.3	10.2	9.65	10.6
La/Sc	3.01	2.94	2.97	2.94	3.13	2.8	3.0	2.71	3.03	3.05	2.84	2.95	2.96	3.15	2.91	2.96
V/Cr	1.85	2.2	2.5	2.54	1.26	1.84	2.02	1.5	2.22	1.94	2.37	2.32	2.48	2.07	2.24	2.09
V/Sc	13.3	13.8	14.8	14.9	14.2	14.3	15.5	6.96	17.6	16.2	17.3	16.9	16.6	16.9	16.4	12.4
Th/Co	0.9	0.86	0.95	0.94	0.81	0.7	0.91	0.76	0.94	0.94	0.95	0.89	0.67	0.98	1.05	0.88
Cu/Zn	0.19	0.7	0.2	0.15	0.52	0.35	0.28	0.63	0.83	1.26	0.26	0.86	0.26	0.16	0.2	0.46
U/Th	0.40	0.5	0.33	0.40	0.50	0.36	0.47	0.82	0.56	0.54	0.42	0.52	0.51	0.64	0.58	0.48
Th/U	2.48	2.0	3.0	2.52	2.0	2.79	2.15	1.22	1.79	1.85	2.38	1.93	1.97	1.57	1.74	2.09

Table 2 (continued)

Sample no.	Sararu section															
	BS.1	BS.2	BS.3	BS.4	BS.5	BS.6	BS.7	BS.8	BS.9	BS.10	BS.11	BS.12	BS.13	BS.14	BS.15	average
Th/Cr	0.11	0.12	0.13	0.13	0.07	0.1	0.1	0.14	0.1	0.09	0.11	0.11	0.12	0.1	0.11	0.11
CIA	79.1	82.1	76.3	85.5	83.5	85.8	84.2	68.6	83.2	79.3	86.1	80.7	79.4	78.3	81.8	81.1
PIA	98.4	98.7	97.7	99.0	98.5	99.0	98.8	96.3	98.5	98.2	99.0	98.7	98.7	98.0	98.7	98.5
ICV	0.71	0.65	0.96	0.59	0.88	0.48	0.61	1.76	0.73	0.99	0.52	0.65	0.67	0.98	0.69	0.76

Sample no.	Sarki section													
	B.1	B.2	B.3	B.4	B.5	B.6	B.7	B.8	B.9	B.10	B.11	B.12	Average	PAAS
SiO_2	13.2	25.7	27.6	25.3	22.4	21.0	14.7	12.1	11.7	23.7	12.3	19.0	19.1	62.4
TiO_2	0.33	0.78	0.64	0.75	0.64	0.42	0.39	0.42	0.25	0.5	0.32	0.48	0.49	0.99
Al_2O_3	12.7	30.9	25.7	23.5	25.4	17.3	15.7	12.8	12.0	21.4	14.0	21.8	19.4	18.78
Fe_2O_3	6.03	11.7	10.9	10.6	10.7	7.52	6.32	6.69	5.69	8.15	5.72	8.69	8.23	7.18
MnO	0.04	0.01	0.02	0.03	0.03	0.04	0.05	0.02	0.04	0.03	0.05	0.04	0.03	0.11
MgO	8.67	5.59	6.86	8.55	9.46	12.1	12.9	0.66	14.5	10.3	13.9	11.0	9.54	2.19
CaO	24.0	4.12	6.52	7.74	7.17	12.1	15.1	35.8	19.1	9.25	17.2	9.76	14.0	1.29
Na_2O	0.14	0.24	0.16	0.24	0.22	0.19	0.16	0.11	0.14	0.19	0.16	0.16	0.18	1.19
K_2O	4.87	11.93	9.37	8.56	9.21	6.29	7.35	2.41	4.24	7.98	6.41	10	7.39	3.68
P_2O_5	0.17	0.12	0.3	0.16	0.24	0.26	0.16	0.21	0.25	0.26	0.17	0.38	0.22	0.16
SO_3	0.08	0.03	0.05	0.05	0.15	0.2	0.38	1.53	0.08	0.05	0.1	0.08	0.23	-
LOI	29.8	8.8	11.8	14.6	14.4	22.6	26.8	27.2	32	18.2	29.6	18.6	21.2	6
Sc	7.1	15.5	12.9	12	12.3	8.7	7.6	7.1	6	10.3	7.5	11.6	9.9	16
V	42	86	82	73	81	58	48	106	44	65	45	72	66.8	150
Cr	18	66	49	48	51	33	30	54	23	43	27	44	40.5	110
Co	3.7	8.1	14.9	8.5	13	9.2	7.7	6.9	5.9	9.4	7.9	8.7	8.7	23
Ni	17.2	29.7	32.5	28.9	34.9	21.9	22.7	53.3	15.9	27.9	22.4	26	27.8	55
Cu	2.1	10.7	18.6	10.5	24.1	12.1	15.5	7.3	8.6	14.4	12.3	18.8	12.9	50
Zn	30	39	39	40	44	32	22	10	28	36	19	35	31.2	85
Rb	79.6	206	138	142	143	91	71	29.2	58.3	112	70.2	94.7	103	160
Sr	122	68	109	115	96	122	100	627	103	88	117	111	148	200
Y	12.7	19.3	20.5	23.3	18.2	14.2	15.7	13.6	9.5	15.5	13.3	14.9	15.8	27
Zr	105	240	214	236	178	123	127	70	80.4	154	85.4	109	143	210
Nb	17.7	40.9	36.3	43.9	29.1	20.3	21.4	10.2	12.3	24.7	14.1	17.4	24	19
Mo	0.6	0.7	0.9	1	0.9	0.6	1.2	12.9	0.9	1.1	1.2	0.8	1.9	-
Ba	70	160	120	110	120	80	70	40	60	90	60	110	90.8	650

757 Page 10 of 23

Table 2 (continued)

Sample no.	Sarki section												Average	PAAS
	B.1	B.2	B.3	B.4	B.5	B.6	B.7	B.8	B.9	B.10	B.11	B.12		
Hf	2.5	6.2	5.8	5.7	4.3	3.1	3.5	1.9	2.0	4.2	2.2	3.0	3.9	5.0
Th	4.0	9.5	8.1	9.5	8.0	4.9	4.2	5.2	3.0	6.3	4.0	6.8	6.1	14.6
U	1.5	2.7	2.6	2.8	2.5	1.9	1.6	2.5	1.6	1.8	1.7	2.3	2.1	3.1
SiO_2/Al_2O_3	1.04	0.83	1.08	1.08	0.88	1.21	0.94	0.94	0.97	1.11	0.88	0.88	0.98	3.32
Al_2O_3/TiO_2	38.5	39.6	40.2	31.3	39.6	41.2	40.1	30.5	48.1	42.8	43.7	45.3	39.7	19.0
K_2O/Na_2O	34.8	49.7	58.6	35.7	41.9	33.1	45.9	21.9	30.3	42.0	40.1	62.5	41.1	3.09
K_2O/Al_2O_3	0.38	0.39	0.36	0.36	0.36	0.36	0.47	0.19	0.35	0.37	0.46	0.46	0.38	0.19
Fe_2O_3/TiO_2	18.3	15.0	17.1	14.1	16.7	17.9	16.2	15.9	22.8	16.3	17.9	18.1	16.8	7.25
Th/Sc	0.56	0.61	0.63	0.79	0.65	0.56	0.55	0.73	0.5	0.61	0.53	0.59	0.61	0.91
Zr/Sc	14.7	15.5	16.6	19.7	14.4	14.1	16.6	9.86	13.4	15.0	11.4	9.4	14.2	13.1
La/Sc	2.59	1.68	2.91	2.5	2.15	2.48	2.58	2.87	2.67	2.37	2.63	2.43	2.49	2.38
V/Cr	2.33	1.3	1.67	1.52	1.59	1.76	1.6	1.96	1.91	1.51	1.67	1.64	1.71	1.36
V/Sc	5.92	5.55	6.36	6.08	6.59	6.67	6.32	14.93	7.33	6.31	6	6.21	6.75	9.38
Th/Co	1.08	1.17	0.54	1.12	0.62	0.53	0.55	0.75	0.51	0.67	0.51	0.78	0.74	0.63
Cu/Zn	0.07	0.27	0.48	0.26	0.55	0.38	0.7	0.73	0.31	0.4	0.65	0.54	0.45	0.59
U/Th	0.38	0.28	0.32	0.30	0.31	0.39	0.38	0.48	0.53	0.29	0.43	0.34	0.36	0.21
Th/U	2.67	3.52	3.12	3.39	3.2	2.58	2.63	2.08	1.88	3.5	2.35	2.96	2.82	4.7
Th/Cr	0.22	0.14	0.17	0.2	0.16	0.15	0.14	0.1	0.13	0.15	0.15	0.15	0.15	0.13
CIA	71.2	71.4	72.7	72.3	72.5	72.2	67.2	83.0	72.8	71.9	67.6	67.9	71.5	75.0
PIA	96.7	97.7	98.2	97.0	97.5	96.8	96.5	98.0	96.7	97.4	96.1	97.5	97.2	87.0
ICV	1.59	0.99	1.09	1.23	1.20	1.54	1.75	0.81	2.07	1.28	1.91	1.40	1.34	0.87

Table 3 Rare earth element concentrations (ppm) for Al-rich shale of the Baluti Formation and Post Archean Australian shale (PAAS) for comparison

Sample no.	Sararu section																
	BS.1	BS.2	BS.3	BS.4	BS.5	BS.6	BS.7	BS.8	BS.9	BS.10	BS.11	BS.12	BS.13	BS.14	BS.15	average
La	22.60	23.80	35.10	29.70	21.60	35.50	19.60	18.70	19.10	18.60	24.40	21.50	24.90	17.00	21.80	23.77
Ce	52.60	52.00	69.80	60.10	48.10	71.80	38.70	39.00	38.40	39.50	49.70	45.40	51.50	35.10	44.20	49.73
Pr	5.65	5.94	8.08	6.85	5.46	8.10	4.40	4.56	4.50	4.53	5.75	5.19	5.99	4.23	5.24	5.70
Nd	22.10	23.50	29.90	27.10	21.50	30.90	16.90	16.70	17.70	17.70	21.70	20.20	23.90	16.80	20.00	22.02
Sm	4.16	4.31	5.59	4.96	4.12	5.55	3.12	3.02	3.29	3.21	4.06	3.78	4.37	3.14	3.82	4.08
Eu	0.77	0.85	1.10	1.02	0.80	1.09	0.60	0.58	0.65	0.67	0.85	0.75	0.90	0.61	0.79	0.81
Gd	3.24	3.41	4.58	4.09	3.24	4.33	2.90	2.73	2.61	2.69	3.41	3.12	3.89	2.48	3.08	3.34
Tb	0.51	0.55	0.70	0.66	0.49	0.72	0.50	0.45	0.40	0.42	0.53	0.47	0.59	0.38	0.50	0.52
Dy	2.92	3.16	4.05	3.79	2.77	4.19	2.99	2.70	2.29	2.36	3.09	2.80	3.41	2.18	2.80	3.02
Ho	0.54	0.59	0.75	0.70	0.51	0.80	0.56	0.52	0.45	0.46	0.58	0.51	0.62	0.41	0.53	0.57
Er	1.57	1.67	2.28	2.03	1.46	2.39	1.70	1.58	1.28	1.34	1.67	1.49	1.79	1.17	1.52	1.65
Tm	0.22	0.23	0.33	0.29	0.21	0.33	0.24	0.22	0.18	0.18	0.24	0.22	0.25	0.16	0.22	0.23
Yb	1.41	1.51	2.13	1.86	1.32	2.26	1.49	1.43	1.10	1.13	1.56	1.38	1.60	1.04	1.34	1.50
Lu	0.22	0.23	0.33	0.29	0.21	0.33	0.24	0.23	0.18	0.19	0.24	0.22	0.25	0.16	0.22	0.23
ΣREE	118.5	121.8	164.7	143.4	111.8	168.3	111.8	92.40	92.10	93.00	117.8	107.0	124.0	84.90	106.1	117.2
$Eu/Eu*_{CN}$	0.64	0.68	0.66	0.69	0.67	0.68	0.70	0.62	0.68	0.70	0.70	0.67	0.67	0.67	0.70	0.68
$(Gd/Yb)_{CN}$	1.86	1.83	1.74	1.78	1.99	1.55	1.89	1.55	1.92	1.93	1.77	1.83	1.97	1.93	1.86	1.83
$(La/Yb)_{CN}$	10.83	10.65	11.14	10.79	11.06	10.61	10.95	8.84	11.73	11.12	10.57	10.53	10.52	11.05	10.99	10.76
$Eu/Eu*_{PN}$	0.99	1.04	1.02	1.07	1.03	1.05	0.94	0.95	1.04	1.07	1.08	1.03	1.03	1.03	1.08	1.03
LREE	107.9	110.4	149.6	129.7	101.6	152.9	101.5	82.60	83.60	84.20	106.5	96.82	111.6	76.88	95.85	106.1
HREE	10.63	11.35	15.15	13.71	10.21	15.35	10.28	9.86	8.49	8.77	11.32	10.21	12.40	7.98	10.21	11.06
LREE/HREE	10.15	9.73	9.87	9.46	9.95	9.96	9.88	8.37	9.85	9.60	9.40	9.48	9.00	9.63	9.39	9.59

Sample no.	Sarki section														
	B.1	B.2	B.3	B.4	B.5	B.6	B.7	B.8	B.9	B.10	B.11	B.12	Ave.	PAAS
La	18.40	26.10	37.60	30.00	26.40	21.60	19.60	20.40	16.00	24.40	19.70	28.20	24.03	38.20
Ce	37.50	51.60	70.10	58.90	53.50	44.30	38.70	43.00	29.60	47.80	38.80	55.20	47.42	79.60
Pr	4.28	5.82	8.19	6.92	6.05	5.06	4.40	5.11	3.45	5.49	4.45	6.18	5.45	8.83
Nd	16.40	20.60	30.40	26.10	22.00	19.50	16.90	19.50	13.20	20.50	16.80	23.80	20.48	33.90
Sm	3.05	3.41	4.61	4.90	4.16	3.50	3.12	3.69	2.32	3.55	2.92	4.18	3.62	5.55
Eu	0.53	0.62	0.88	0.95	0.78	0.65	0.60	0.73	0.40	0.67	0.55	0.84	0.68	1.08
Gd	2.53	3.10	4.27	4.50	3.65	2.95	2.90	2.86	1.99	3.24	2.62	3.53	3.18	4.66
Tb	0.40	0.52	0.71	0.75	0.60	0.47	0.50	0.47	0.31	0.54	0.43	0.51	0.52	0.77
Dy	2.29	3.21	4.11	4.52	3.51	2.88	2.99	2.62	1.79	2.93	2.33	2.99	3.01	4.68
Ho	0.45	0.63	0.82	0.86	0.69	0.52	0.56	0.49	0.35	0.57	0.50	0.57	0.58	0.99
Er	1.30	2.00	2.33	2.56	2.09	1.47	1.70	1.53	1.00	1.73	1.43	1.64	1.73	2.85
Tm	0.19	0.30	0.34	0.38	0.28	0.23	0.24	0.19	0.14	0.24	0.21	0.23	0.25	0.41

Table 3 (continued)

Sample no.	Sarki section												Ave.	PAAS
	B.1	B.2	B.3	B.4	B.5	B.6	B.7	B.8	B.9	B.10	B.11	B.12		
Yb	1.26	1.94	2.26	2.58	1.84	1.39	1.49	1.30	0.93	1.64	1.34	1.57	1.63	2.82
Lu	0.19	0.32	0.38	0.40	0.28	0.22	0.24	0.20	0.15	0.27	0.22	0.25	0.26	0.43
ΣREE	88.77	120.2	167.0	144.3	125.8	104.7	93.94	102.1	71.6	113.6	92.30	129.7	112.8	184.8
Eu/Eu*$_{CN}$	0.58	0.58	0.61	0.62	0.61	0.62	0.61	0.69	0.57	0.60	0.61	0.67	0.61	0.71
(Gd/Yb)$_{CN}$	1.63	1.30	1.53	1.41	1.61	1.72	1.58	1.78	1.73	1.60	1.58	1.82	1.61	1.34
(La/Yb)$_{CN}$	9.87	9.09	11.24	7.86	9.70	10.50	8.89	10.6	11.63	10.05	9.93	12.14	10.13	9.15
Eu/Eu*$_{PN}$	0.90	0.90	0.93	0.95	0.94	0.95	0.94	1.06	0.88	0.93	0.94	1.03	0.94	-
LREE	80.16	108.2	151.8	127.8	113.0	94.60	83.30	92.40	65.00	102.4	83.20	118.4	101.7	167.2
HREE	8.61	12.02	15.22	16.55	12.94	10.13	10.62	9.66	6.66	11.16	9.08	11.29	11.16	17.61
LREE/HREE	9.31	9.00	9.97	7.72	8.72	9.34	7.85	9.57	9.76	9.18	9.17	10.49	9.11	9.49

positive correlation of REE with SiO_2, Al_2O_3, and TiO_2 (Table 4) indicates that the REEs are controlled mainly by clay minerals in the shale.

Transition trace elements (Sc, V, Cr, Co, Ni, Cu, and Zn)

As observed for the great majority of the other trace elements, the transition trace element (TTE) contents of the studied shales are also depleted relative to those of the PAAS (Table 2). However, the higher concentrations of Cr (58.1 ppm on average) in the shale of the Sararu section indicate a proportion of mafic rocks in their source area (Taylor and McLennan 1985; Wronkiewicz and Condie 1990). The Th/Cr ratio, a good indicator for provenance (Condie and Wronkiewicz 1990), has average values of 0.106 and 0.148 in the Sararu and Sarki shales, respectively (Table 2). In general, most of the TTEs in the Baluti shale are positively correlated with Al_2O_3 and TiO_2 (Table 4), indicating that they are mainly concentrated in the phyllosilicates.

Rare earth elements

Concentration of rare earth elements from La to Lu are significantly lower in studied shale compared with those of PAAS, and are nearly similar in the studied sections (Table 3). The results suggest that the major control over the REE concentrations is the dilution effect caused mostly by carbonate (correlation coefficient between CaO and ΣREE is −0.608 for the Sarki section).
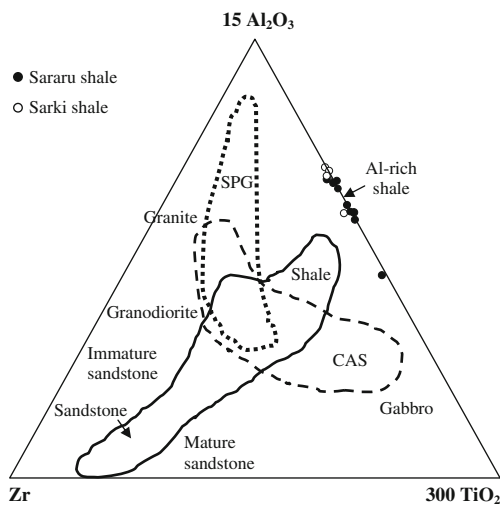
Chondrite and PAAS-normalized REE patterns are given in Fig. 5 indicating LREE enrichment with higher $(La/Yb)_{CN}$ ratios (10.76 and 10.13 for Sararu and Sarki, respectively) relative to PAAS (9.15), and slight to moderate negative Eu anomalies ($Eu/Eu*_{CN}$ is 0.68 and 0.61 in Sararu and Sarki, respectively). The mean REEs are depleted relative to the PAAS (Fig. 5a–c). The patterns show enrichment in light REE (LREE) and depletion in heavy REE (HREE) in addition to flat HREE pattern. The significant correlation of REE with Al_2O_3, TiO_2, Th, and Zr indicates that REE distribution is likely controlled by the collective influence of phyllosilicate, zircon, and opaque phases. The Baluti shales have highly enriched LREE patterns where $(La/Sm)_{CN} = 3.67$ and 4.18 for Sararu and Sarki, respectively; moreover, these are slightly lower than PAAS (4.33; Taylor and McLennan 1985). The studied shale has flat to moderately fractionated HREE patterns which $(Gd/Yb)_{CN} = 1.83$ and 1.61 for Sararu and Sarki, respectively (Fig. 5a–c; Table 3). Weak negative and no Ce anomalies ($Ce/Ce*_{PN}$) for Sararu shale (0.95–1.07; average 0.99) and weak for Sarki (0.92–0.98; average = 0.96)

Table 4 Correlation matrix for the shale from the Baluti Formation, Sararu and Sarki sections

	SiO_2	Al_2O_3	Fe_2O_3	CaO	MgO	Na_2O	K_2O	MnO	TiO_2	P_2O_5	SO_3	LOI	Rb	Sr	Ba	Th	U	Y	Zr	Nb	Mo	Hf	Sc	V	Cr	Co	Ni	Cu	Zn	REE
SiO_2	1																													
Al_2O_3	.260	1																												
Fe_2O_3	.234	-.059	1																											
CaO	-.621	-.468	-.115	1																										
MgO	.153	-.073	-.053	-.754	1																									
Na_2O	.483	.167	.152	-.910	.876	1																								
K_2O	.431	.213	-.075	-.861	.825	.886	1																							
MnO	.117	.155	.223	-.705	.775	.774	.684	1																						
TiO_2	.654	.772	.263	-.397	-.279	.152	.136	.020	1																					
P_2O_5	-.374	-.183	.112	.639*	-.620	-.672	-.540	-.327	-.083	1																				
SO_3	-.599	-.505	.109	.512	-.122	-.255	-.304	-.215	-.526	.425	1																			
LOI	-.767	-.684	-.289	.472	.188	-.247	-.251	.031	-.953	.164	.453	1																		
Rb	.615	.462	.036	-.960	.719	.921	.894	.672	.443	-.672	-.495	-.506	1																	
Sr	-.387	-.334	.147	.820	-.726	-.745	-.890	-.562	-.147	.564	.389	.255	-.787	1																
Ba	.702	.483	.158	-.808	.448	.732	.661	.371	.615	-.610	-.411	-.694	.872	-.546	1															
Th	.659	.737	.259	-.334	-.346	.075	.080	-.072	.989	-.060	-.516	-.957	.379	-.104	.594	1														
U	.375	.497	.031	-.700	.438	.535	.649	.381	.329	-.180	-.348	-.401	.650	-.687	.561	.312	1													
Y	.689	.671	.286	-.448	-.161	.228	.212	.082	.933	-.227	-.583	-.901	.512	-.167	.727	.945	.312	1												
Zr	.834	.525	.331	-.813	.333	.706	.637	.467	.771	-.472	-.535	-.822	.706	-.545	.738	.515	.819	1												
Nb	.709	.632	.172	-.924	.506	.803	.748	.601*	.684	-.564	-.584	-.709	.949	-.670	.897	.626	.624	.721	.947	1										
Mo	-.057	.215	-.118	.143	-.317	-.321	-.008	-.110	.161	.567	-.122	-.118	-.156	-.035	-.219	.204	.369	.132	-.076	-.096	1									
Hf	.751	.725	.211	-.813	.275	.630	.611	.438	.841	-.448	-.631	-.852	.844	-.568	.856	.798	.558	.852	.957	.962	-.009	1								
Sc	.710	.750	.271	-.481	-.176	.248	.225	.067	.983	-.217	-.564	-.962	.533	-.219	.717	.981	.366	.972	.838	.751	.105	.888	1							
V	.469	.650	.250	-.035	-.613	-.224	-.199	-.246	.907	.262	-.346	-.839	.063	.129	.287	.929	.171	.790	.346	.361	.559	.845	.723	1						
Cr	.269	.620	.332	-.054	-.458	-.106	-.241	-.148	.763	.047	-.269	-.649	.092	.253	.292	.745	-.003	.716	.395	.331	.130	.485	.723	.743	1					
Co	.487	.813	.141	-.418	-.175	-.204	.251	.090	.896	-.184	-.500	-.844	.499	-.263	-.608	.893	.425	.896	.716	.678	.333	.801	.910	.786	.761	1				
Ni	.256	.552	.221	.161	-.707	-.345	-.309	-.368	.782	.367	-.156	-.708	-.076	.355	.178	.814	.079	.695	.314	.175	.421	.382	.721	.910	.779	.743	1			
Cu	.022	.428	.402	-.222	.001	.218	.016	.207	.394	-.129	-.034	-.311	.249	.093	.322	.347	.122	.438	.312	.346	.012	.359	.405	.264	.787	.556	.397	1		
Zn	.427	.460	.319	-.217	.048	-.032	-.163	.596				-.071	-.090	-.661	.200	.109	.174	.650	.463	.366	.177	.451	.629	.570	.647	.612	.619	.518	1	
REE	.671	.672	.257	-.348	-.284	.126	.117	-.046	.955	-.179	-.550	-.924	.424	-.088	.659	.970	.228	.986	.765	.648	.118	.809	.978	.846	.755	.893	.763	.409	.648	1

0.647 significant at 0.01 level   0.515 significant at 0.05 level   no of samples= 15

	SiO_2	Al_2O_3	Fe_2O_3	CaO	MgO	Na_2O	K_2O	MnO	TiO_2	P_2O_5	SO_3	LOI	Rb	Sr	Ba	Th	U	Y	Zr	Nb	Mo	Hf	Sc	V	Cr	Co	Ni	Cu	Zn	REE
SiO_2	1																													
Al_2O_3	.914	1																												
Fe_2O_3	.914	.967	1																											
CaO	-.827	-.831	-.741	1																										
MgO	-.237	-.284	-.406	-.279	1																									
Na_2O	.755	.788	.755	-.808	.035	1																								
K_2O	.794	.916	.815	-.914	.030	.753	1																							
MnO	-.599	-.654	-.723	.189	.815	-.330	-.337	1																						
TiO_2	.881	.930	.968	-.671	-.473	.796	.768	-.724	1																					
P_2O_5	.149	.055	.059	-.153	.148	-.271	.093	.078	-.128	1																				
SO_3	-.433	-.404	-.298	.776	-.621	-.532	-.610	-.205	-.208	-.089	1																			
LOI	-.950	-.984	-.981	.780	.376	-.752	-.857	.700	-.952	-.104	.315	1																		
Rb	.860	.944	.903	-.837	-.182	.866	.882	-.591	.884	-.167	-.556	-.901	1																	
Sr	-.401	-.391	-.262	.793	-.686	-.545	-.628	-.280	-.181	-.032	.971	.290	-.537	1																
Ba	.852	.967	.922	-.852	-.179	.786	.938	-.573	.867	.032	-.540	-.924	.966	-.523	1															
Th	.877	.931	.971	-.671	-.469	.762	.779	-.713	.988	-.019	-.223	-.957	.862	-.173	.869	1														
U	.671	.744	.855	-.362	-.662	.503	.510	-.774	.870	.046	.144	-.802	.610	.211	.648	.893	1													
Y	.839	.810	.869	-.644	-.365	.725	.697	-.522	.929	-.157	-.226	-.855	.764	-.212	.732	.912	.786	1												
Zr	.907	.897	.913	-.778	-.268	.828	.786	-.606	.936	-.208	-.439	-.902	.926	-.424	.871	.902	.689	.91	1											
Nb	.881	.860	.886	-.757	-.249	.830	.758	-.563	.924	-.246	-.442	-.868	.902	-.424	.839	.889	.679	.930	.995	1										
Mo	-.369	-.339	-.223	.756	-.700	-.503	-.581	-.323	-.135	-.066	.976	-.484	-.132	.238	-.179	-.380	-.386				1									
Hf	.922	.911	.910	-.788	-.277	.781	.811	-.620	.926	-.156	-.421	-.917	.915	-.416	.874	.893	.677	.910	.991	.978	-.366	1								
Sc	.893	.992	.967	-.792	-.336	.757	.910	-.670	.934	.064	-.378	-.979	.933	-.347	.967	.945	.779	.812	.879	.847	-.302	.892	1							
V	.445	.523	.623	-.018	-.855	.171	.225	-.828	.639	.124	.528	-.606	.319	.570	.372	.657	.860	.497	.379	.342	.607	.400	.553	1						
Cr	.665	.791	.819	-.367	-.692	.503	.561	-.852	.842	.002	.214	-.824	.637	.232	.667	.845	.898	.673	.643	.603	.295	.666	.803	.908	1					
Co	.715	.652	.675	-.614	-.102	.364	.552	-.349	.563	.417	-.195	-.693	.481	-.202	.528	.573	.540	.598	.545	.500	-.174	.584	.612	.445	.512	1				
Ni	.160	.216	.329	.281	-.839	-.074	-.080	-.636	.385	.030	.764	-.314	.002	.784	.024	.394	.664	.315	.112	.084	.819	.132	.240	.917	.724	.328	1			
Cu	.489	.549	.501	-.624	.186	.341	.605	-.022	.383	.499	-.248	-.534	.352	-.321	.465	.412	.335	.396	.325	.278	-.280	.365	.502	.257	.374	.839	.167	1		
Zn	.822	.792	.783	-.866	.090	.759	.770	-.331	.687	.217	-.731	-.771	.828	-.691	.842	.704	.419	.612	.771	.751	-.680	.744	.765	.099	.346	.533	-.218	.476	1	
REE	.851	.781	.848	-.608	-.390	.462	.664	-.541	.810	.312	-.202	-.854	.633	-.136	.692	.848	.792	.863	.758	.747	-.126	.782	.801	.585	.658	.779	.380	.545	.620	1

0.700 significant at 0.01 level   0.581 significant at 0.05 level   no of samples= 12

as shown in Fig. 5d–f. Europium in Sararu shale generally exhibit positive, with some samples showing negative, anomalies (Fig. 5d, f) with an average ($Eu_n/Eu_{n\ PN}^*$) = 1.03 and the Sarki shale shows negative anomalies in REE distribution patterns (Fig. 5e, f) with an average $Eu_n/Eu_n^* = 0.94$.

Fig. 4 Al–Ti–Zr ternary diagram (wt%) for the shale of the Baluti Formation (fields after Garcia et al. 1994). SPG is strongly peraluminous granite and CAS is calc-alkaline suites

Discussion

Clay mineralogy

Baluti shales at Sararu section yield clay mineral assemblage dominated by illite and kaolinite with occurrences of mixed layer illite/smectite. Neither chlorite nor discrete smectite were found in the Sararu shales. At the Sarki section, the clay assemblage is found to be dominated by illite with subordinate quantities of smectite and sporadic occurrence of kaolinite. Kaolinite has been accepted for a long time as a product of chemical weathering. Kaolinite formation is, therefore, favored under tropical to subtropical humid climatic conditions (Chamley 1989; Hallam et al. 1991). In addition to the detrital origin, kaolinite may also develop by diagenetic processes that is indicated by the Al enrichment of the studied shale.

Illite typically is formed under conditions completely different from those under which kaolinite and smectite were formed. Illite is typically formed in soils with little chemical weathering in cold and/or dry climates, and in areas of high relief where physical erosion is predominant. Illite has no climatic significance; however, low illite crystallinity index may attribute to cold or dry climate conditions with minimum hydrolysation (Singer 1984; Ghandour et al. 2003) as in illite of Sarki section. The relative abundance of kaolinite to smectite is clearly influenced by hydraulic sorting and relative sea level changes. Kaolinite tends to concentrate in sediments of non-marine and marginal marine settings, whereas smectite is reported to have higher relative abundance from normal marine shales. This could be attributed to the hydraulic segregation of clay minerals (Raucsik and Merényi 2000). Smectite, on the other hand, favors conditions of pronounced dry seasons alternating with less-pronounced wet seasons (Singer 1984). Numerous mineralogical and chemical studies of

smectitic minerals suggest that smectite from most Mesozoic sediments are mainly soil-derived minerals (Chamley 1989; Ghandour et al. 2003). Smectite may be volcanogenic in origin (Hallam et al. 1991), being derived directly from the weathering and alteration of volcanic materials. Kaolinite crystallinity and illite chemistry indices in Sarki samples are higher than that of Sararu; these reflect the well kaolinite crystallinity and Al-rich (muscovitic) illite in the Sararu samples. Accordingly, it may suggest that the Sararu shale was deposited under tropical to subtropical and the Sarki shale deposited under drier climate.

Palaeoweathering conditions

Alteration of the rocks during weathering resulted in depletion of alkali and alkaline earth elements and preferential enrichment of Al_2O_3 (Nesbitt et al. 1980). Consequently, the weathering condition can be measured in terms of the molecular percentage of the oxide components, using the indexes of CIA, PIA, and ICV (Hu et al. 2015). Since there is no direct method to distinguish and quantify the contents of CaO belonging to silicate fraction and non-silicate fraction (carbonates and apatite), we used in this study the method reported by McLennan et al. (1993) to calculate the CaO in silicate fraction is used in current study; the molar proportion of Na_2O is taken as the molar proportion of CaO of the silicate fraction.

The chemical index of alternation (CIA) is one of the most widely used indexes with higher values suggesting more intense chemical weathering (Armstrong-Altrin et al. 2004).

$$CIA = \left[Al_2O_3 / \left(Al_2O_3 + CaO^* + Na_2O + K_2O \right) \right] \times 100$$

(Nesbitt and Young 1982).

In general, CIA values close to 100 are due to more intense weathering which produces residual clays enriched in kaolinite and Al oxy-hydroxides. Different parent materials have different initial CIA values. For example, basalts have a CIA of <45 (Sheldon 2003), felsic rocks 55–60, and shales 70–75 (Nesbitt and Young 1982; Maynard 1992).

The CIA values in Baluti shale vary from 68.90 to 86.08 (average = 81.11) in the Sararu section and from 67.15 to 83.03 (average = 71.53) in the Sarki section. The former average is higher than PAAS (=75; Taylor and McLennan 1985) and the latter is lower; this implies that the Baluti Formation sedimentary rocks suffered intense degree of weathering for Sararu, and high to moderate for Sarki. Nesbitt and Young (1982) and Nyakairu and Koeberl (2001) used a ternary diagram Al_2O_3–CaO + Na_2O–K_2O (A–CN–K) to infer the weathering history at the source area. The studied samples plot in a tight group on the A–K join, and close to the muscovite point for Sarki shale and close to illite point for Sararu shale (Fig. 6).
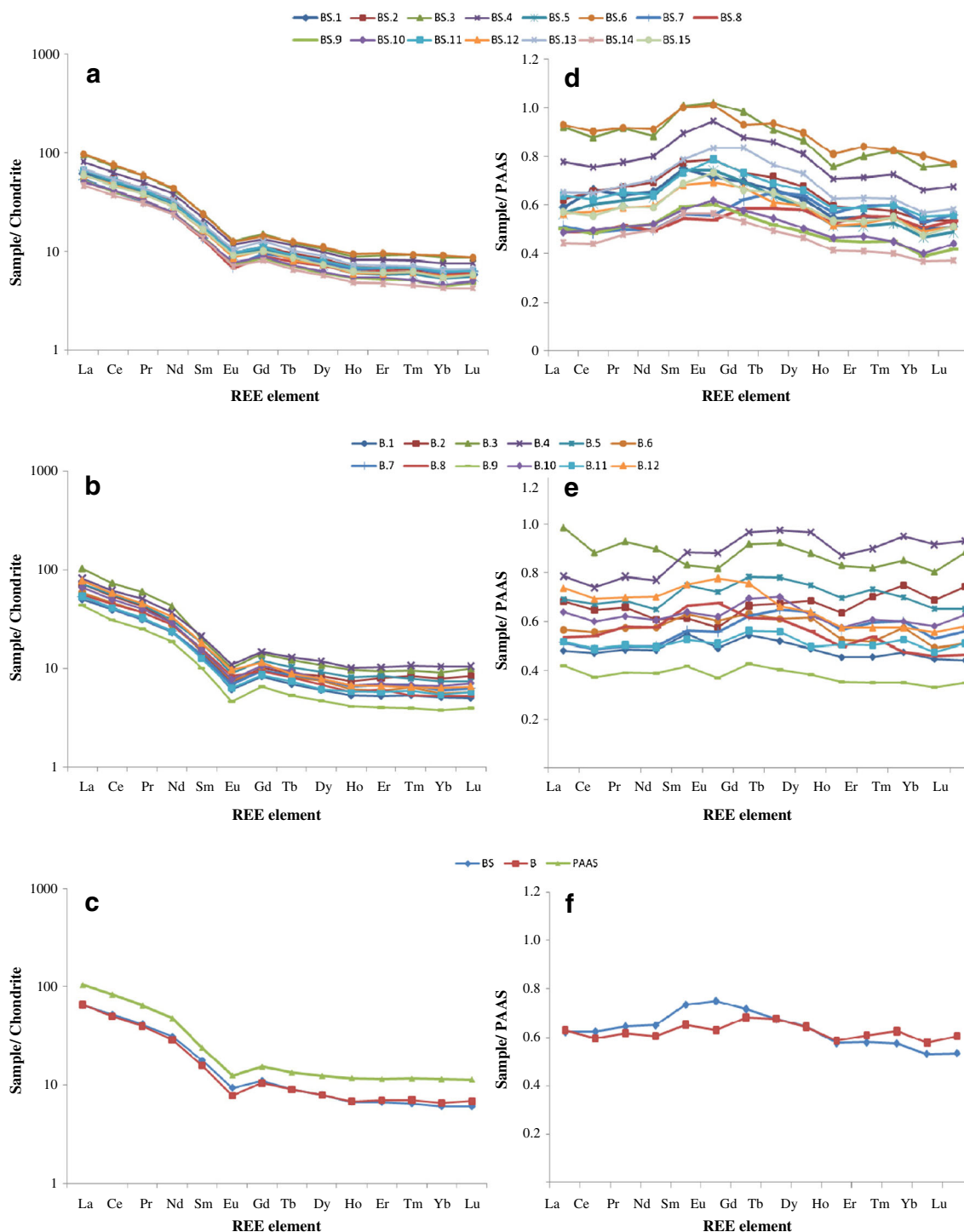
Fig. 5 Chondrite and PAAS normalized rare earth elements plot for shale samples from the Baluti Formation. **a–c** Chondrite-normalized. **d–f** PAAS-normalized. Chondrite and PAAS normalization values are from Taylor and McLennan (1985)

In addition, plagioclase index of alteration (PIA) and index of compositional variation (ICV) can also provide indication of the degree of weathering in the source region.
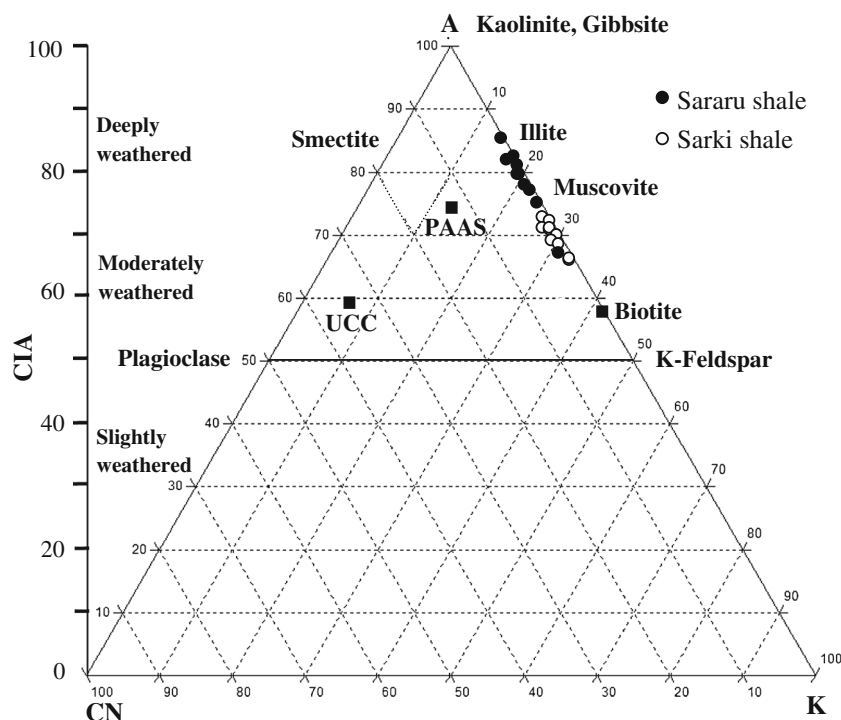
(Fedo et al. 1995)

$$ICV = (CaO + K_2O + Na_2O + Fe_2O_3 + MgO + MnO + TiO_2)/Al_2O_3$$

$$PIA = \left[(Al_2O_3 - K_2O) / \left(Al_2O_3 + CaO^* + Na_2O - K_2O \right) \right] \times 100$$

(Cox et al. 1995)

Fig. 6 A-CN-K ternary diagram in molecular proportions for the Baluti shale (after Nesbitt and Young 1984). Also plotted is the average Upper Continental Crust and Post Archean Australian Shale (Taylor and McLennan 1985)

The maximum value of PIA is 100 for completely altered materials and weathered plagioclase has a PIA value of 50. PIA values for Baluti shale range from 96.28 to 99.01 (average = 98.52) in Sararu and from 96.14 to 98.17 (average = 97.23) in Sarki, which suggest intense plagioclase weathering in the source area.

The ICV (Cox et al. 1995) is potentially useful to evaluate the degree of chemical weathering, which depicts formation of aluminous clay minerals over the framework silicate minerals. Moreover, the sediments with ICV > 1 are compositionally immature with the first cycle of sediments deposited in tectonically active settings. On the other hand, those with ICV < 1 are compositionally mature and are deposited in a tectonically quiescent or cratonic environment where sediment recycling is active (Weaver 1989; Cox et al. 1995). The ICV values for the Baluti shale vary from 0.48 to 1.76 (average = 0.76) at Sararu and from 0.81 to 2.07 (average = 1.34) at Sarki. On the basis of average ICV values, it can be interpreted that the shale at Sararu is compositionally mature and deposited in tectonically quiescent or cratonic environment; whereas, it is compositionally less mature and deposited in tectonically active settings at Sarki. Thus, the variability in ICV values may be due to both variations in source-rock composition and differences in weathering (Potter et al. 2005).

Provenance

The geochemical signatures of clastic sediments are frequently used to infer their provenance characteristics, because they reflect the source rock composition, hydraulic sorting during transport, deposition, and diagenesis (Taylor and McLennan 1985; Condie et al. 1992; Cullers 1995; Madhavaraju and Ramasamy 2002; Armstrong-Altrin et al. 2004; Nagarajan et al. 2007; Shadan and Hosseini-Barzi 2013; Absar and Sreenivas 2015). The trace elements concentrated in mafic (Sc, Cr and Co) and in silicic (La, Th, and REE) sediments, the REE patterns and the size of the Eu anomaly are considered as important tools to characterize the source rock composition (e.g., Cullers et al. 1979; Garver and Scott 1995; Girty et al. 1996; Armstrong-Altrin et al. 2004; Shynu et al. 2013; Zaid and Gahtani 2015; Dai et al. 2016).

Al_2O_3/TiO_2 ratios of most clastic rocks are essentially used to infer the source rock compositions because the Al_2O_3/TiO_2 ratio increases from 3 to 8 for mafic igneous rocks, from 8 to 21 for intermediate rocks, and from 21 to 70 for felsic igneous rocks (Hayashi et al. 1997). In the Sararu shales, the Al_2O_3/TiO_2 ratio ranges from 17.81 to 38.86 and in Sarki shales it varies between 30.52 and 48.12 (Table 2). Thus, the Al_2O_3/TiO_2 ratio of this study suggests that felsic-intermediate igneous rocks were the probable source rocks for the shales of the Baluti Formation.

Taylor and McLennan (1985) and McLennan and Taylor (1991) suggest that the REEs, Th, Sc, Co, Ti, and HFSEs (Zr, Hf) are especially useful for monitoring source area composition. These elements have very short residence times in seawater and are transferred almost quantitatively into the sedimentary record. Additionally, this includes both incompatible (Th, REEs, HFSEs) and compatible elements (Sc, Co, Ti),

ratios of which are useful in differentiating felsic from mafic source components. However, the ratios such as La/Sc, Th/Sc, Th/Cr, Th/Co, Eu/Eu*$_{CN}$, and Eu/Eu*$_{PN}$ are significantly different in felsic and basic rocks and may allow constraints on the average provenance composition (Wronkiewicz and Condie 1990; Cox et al. 1995; Cullers 1995; Dai et al. 2016). The ratios of the studied shales are compared with those of sediments derived from felsic and basic rocks as well as to Upper Continental Crust (UCC) and PAAS values (Table 5). These ratios for Sararu are higher than that for Sarki shale (except Th/Cr), and the comparison suggests that these ratios are within the range of felsic rocks. Th/Sc–Zr/Sc diagram (McLennan et al. 1993) shows that the samples of the Baluti shale are clustered between felsic volcanic and granodiorite and it is clear that the Sararu samples are clustered toward the intermediate rocks (Fig. 7).

The provenance of Baluti Formation is carried out based on the concentrations of some elements, ratios, and plotting on the diagrams. Floyd and Leveridge (1987) plot K_2O versus Rb to distinguish between the sediments derived from acidic to intermediate rocks and those derived from basic rocks. Most of the studied shale of the Baluti Formation lies in the field of acid and intermediate compositions with some samples of Sararu shale that falls in the basic field (Fig. 8).

The other bivariate plot to discriminate provenance is La/Th versus Hf (Floyd and Leveridge 1987; Gu et al. 2002; Spalletti et al. 2012) that is useful for providing source areas composition. The average La/Th values of the shale from Sararu and Sarki sections are 3.84 and 4.14, respectively (Table 2). The samples in both sections show higher values in respect to PAAS (2.61) and UCC (2.8). The studied samples are scattered in the felsic toward the andesitic field (Fig. 9).

The chondrite and PAAS-normalized REE patterns and Eu anomaly in the sedimentary rocks provide important clues regarding the source rock characteristics (Taylor and McLennan 1985). The REE distribution patterns for the two studied sections are similar to that of the average PAAS and UCC (Taylor and McLennan 1985). The REE patterns for
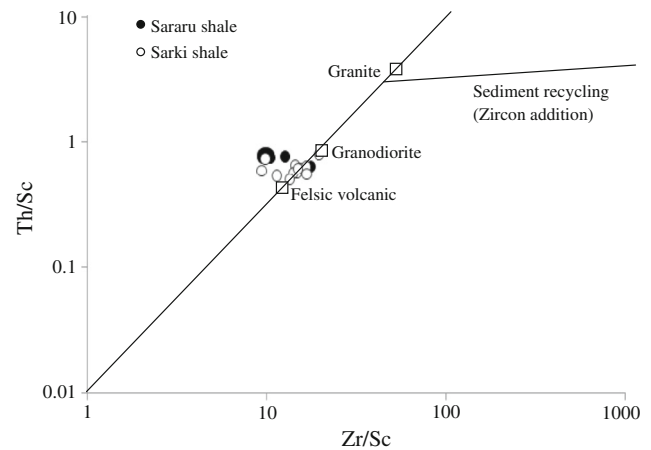
Fig. 7 Th/Sc–Zr/Sc diagram (McLennan et al. 1993) shows that sandstone and shale cluster around average granite with minor contribution from granodiorite. Values of granite, granodiorite, and felsic volcanic are after Condie (1993)

Sararu and Sarki nearly coincide except for smaller negative Eu anomaly size for Sararu shale (Fig. 5a–c). Higher LREE/HREE ratios and negative Eu anomalies are generally found in felsic rocks, whereas the mafic rocks exhibit lower LREE/HREE ratios and no or small Eu anomalies (Cullers 1994). The Baluti shales show LREE enriched and flat HREE patterns with negative Eu anomalies (Fig. 5a–c). However, the Baluti shales show high LREE/HREE ratios (9.59 and 9.11 for Sararu and Sarki sections, respectively) and negative Eu anomaly (Eu/Eu*$_{CN}$; 0.68 and 0.61 for the Sararu and Sarki sections, respectively). This suggests that these sedimentary rocks were mainly derived from the felsic source rocks. The (Gd/Yb)$_{CN}$ ratios (1.83 and 1.61 for Sararu and Sarki sections, respectively) of Baluti shales are less than 2, which suggests that these shales were derived from the less HREE-depleted source rocks (Nagarajan et al. 2007). The similar chondrite-normalized REE patterns (except the Eu anomalies) of Sararu and Sarki shales (Fig. 5a–c) suggest that both sediment groups were likely derived from the same source regions. Cerium in Sararu shale exhibits very weak negative or no anomalies

Table 5 Elemental ratios for the Al-rich shale of the Baluti Formation compared with those of fine-fractions derived from felsic and mafic source rocks

Elemental ratio	Average of studied shale		Range of sediments[a]		UCC[b]	PAAS[b]
	Sararu	Sarki	Felsic rocks	Mafic rocks		
Eu/Eu*	0.68	0.61	0.40–0.94	0.71–0.95	0.65	0.71
Th/Sc	0.77	0.61	0.84–20.50	0.05–0.22	0.79	0.90
Th/Co	0.88	0.74	0.67–19.40	0.04–1.40	0.63	0.63
Th/Cr	0.11	0.14	0.13–2.70	0.018–0.046	0.30	0.13
Cr/Th	9.46	6.74	4.00–15.00	25.00–500	3.30	7.53
La/Sc	2.96	2.49	2.50–16.30	0.43–0.86	2.21	2.40

UCC Upper Continental Crust, *PAAS* Post Archean Australian Shale

[a] Cullers (1994); Cullers and Podkovyrov (2000); Cullers et al. (1988)

[b] Taylor and McLennan (1985)
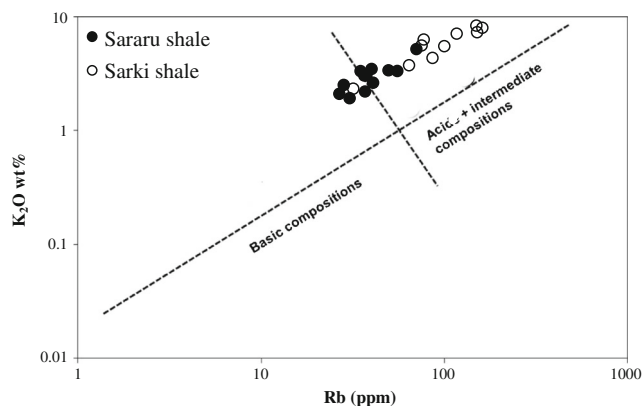
Fig. 8 K_2O versus Rb diagram of the shale of the Baluti Formation (fields after Floyd and Leveridge 1987)

(Fig. 5d, f) and in Sarki has weak negative anomalies (Fig. 5e, f). Several factors, including the rocks in the source area, groundwater or hydrothermal leaching, seawater, and Fe–Mn oxyhydroxide mineralization, may control the Ce anomaly (Dai et al. 2016). The geochemical composition of the source rock is one of the important factors controlling the Ce anomaly. Xiao et al. (2004) suggest the source rock dominated by basalts do not show a Ce anomaly and Dai et al. (2016) consider the source rock dominated by felsic and felsic-intermediate rocks are characterized by weakly negative Ce anomalies, and the shales with input from these terrigenous materials usually have weak Ce anomalies. Source rocks comprising mafic basalt are characterized by strong positive Eu anomalies (Xiao et al. 2004) and thus shales with input from these terrigenous materials have positive Eu anomalies Eu/Eu*$_{PN}$. Shale with input of felsic-intermediate terrigenous materials usually displays distinct negative Eu anomalies. Accordingly, the different shape of PAAS-normalized patterns (shape of Ce anomaly and Eu anomaly; Fig. 5d–f) may suggest the felsic-intermediate source rock for the studied shales with influence of the Sararu shale by mafic rocks.
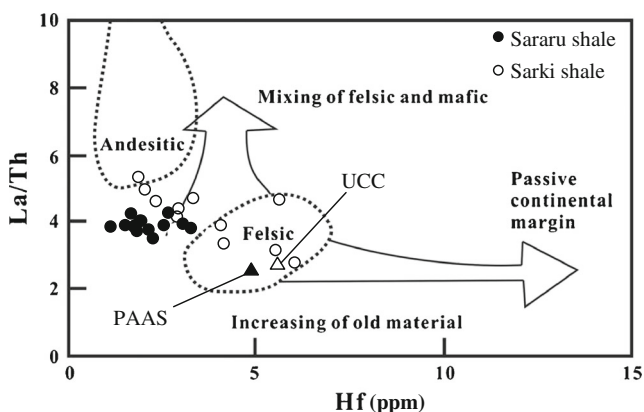
Fig. 9 La/Th versus Hf diagram for the shale of the Baluti Formation (fields after Floyd and Leveridge 1987)

Based on these geochemical data, it is suggested that the shale of the Sarki succession was derived from the Arabian Shield and Rutba Uplift. It was exposed to southwest of the studied area and no volcanism was occurring during the deposition. However, the Sararu succession was fed from the Arabian Shield and Rutba Uplift and exposed to the southwest; some sediment were derived from the Bitlis-Avroman-Bisitoun Ridge that contain some occurrence of volcanic rocks located to the north and northeastern of the basin (Fig. 1b). Surdashy (2012) suggest the south direction for paleo-current during the Upper Triassic.

Tectonic setting

The chemical composition of the source rock is a function of the tectonic setting and exerts major control on the chemistry of sedimentary rocks. Therefore, it can be directly related to plate tectonic processes and it has been traditionally used to identify their tectonic setting of unidentified basins (Taylor and McLennan 1985; Roser and Korsch 1986; McLennan and Taylor 1991; Girty and Barber 1993; Purevjav and Roser 2012; Yan et al. 2012). Nevertheless, in recent years, tectonic discrimination depends on major elements that has received considerable criticism (Armstrong-Altrin and Verma 2005; Ryan and Williams 2007; Verma and Armstrong-Altrin 2013; Tobia and Shangola 2016). Trace elements, particularly those that are relatively immobile with low residence times in seawater (i.e., La, Nd, Th, Zr, Hf, Nb, and Ti) are reliable fingerprints for tectonic setting discrimination (McLennan et al. 1990; Gu 1996; LaMaskin et al. 2008).

Verma and Armstrong-Altrin (2013) proposed two discriminant functions based on major elements for the tectonic discrimination of siliciclastic sediments. The three main tectonic settings are: island or continental arc, continental rift, and collision. The tectonic discrimination depends on the silica contents; high silica (SiO_2 = 63–95 %) and low silica rocks (SiO_2 = 35–63 %). These two diagrams were constructed based on worldwide examples of Neogene-Quaternary siliciclastic sediments from known tectonic settings. The diagrams were evaluated by Armstrong-Altrin et al. (2014) who suggested that these diagrams can be measured as a successful tool for discriminating the tectonic setting of older sedimentary basins, which may consist of one or more tectonic assemblages. The discriminant function based on major elements of low silica diagram was used for the studied samples of the Baluti Formation (Fig. 10). Most of the Sararu samples fell in the rift (passive continental margin) field and of the Sarki in the collision (active continental margin) field.

A number of studies have used the REE distribution in sediments to determine or infer their plate tectonic settings (e.g., Bhatia and Crook 1986; McLennan et al. 1990; McLennan and Taylor 1991; Girty and Barber 1993; Mader and Neubauer 2004; Verma and Armstrong-Altrin 2013). These studies show that sediments deposited in the continental
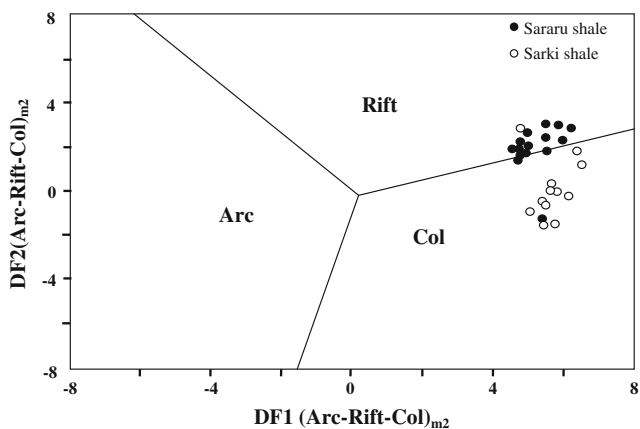
Fig. 10 Discriminant function diagrams for low-silica shale samples of the Baluti Formation (boundaries after Verma and Armstrong-Altrin 2013). Discriminant function equations are: DF1(Arc-Rift-Col)m² = $(0.608 \times \ln(TiO_2/SiO_2)_{adj}) + (-1.854 \times \ln(Al_2O_3/SiO_2)_{adj}) + (0.299 \times \ln(Fe_2O_3^t/SiO_2)_{adj}) + (-0.550 \times \ln(MnO/SiO_2)_{adj}) + (0.120 \times \ln(MgO/SiO_2)_{adj}) + (0.194 \times \ln(CaO/SiO_2)_{adj}) + (-1.510 \times \ln(Na_2O/SiO_2)_{adj}) + (1.941 \times \ln(K_2O/SiO_2)_{adj}) + (0.003 \times \ln(P_2O_5/SiO_2)_{adj}) - 0.294$. DF2(Arc-Rift-Col)m² = $(-0.554 \times \ln(TiO_2/SiO_2)_{adj}) + (-0.995 \times \ln(Al_2O_3/SiO_2)_{adj}) + (1.765 \times \ln(Fe_2O_3t/SiO_2)_{adj}) + (-1.391 \times \ln(MnO/SiO_2)_{adj}) + (-1.034 \times \ln(MgO/SiO_2)_{adj}) + (0.225 \times \ln(CaO/SiO_2)_{adj}) + (0.713 \times \ln(Na_2O/SiO_2)_{adj}) + (0.330 \times \ln(K_2O/SiO_2)_{adj}) + (0.637 \times \ln(P_2O_5/SiO_2)_{adj}) - 3.631$

margin are characterized by LREE enrichment (indicated by high La/Sm) and high total rare earth elements (ΣREE), on the other hand, those from young undifferentiated oceanic arcs have lower La/Sm, lower ΣREE, and lack for Eu anomaly. Therefore, the REE patterns of sediments deposited in continental margins can generally be differentiated from those

derived from undifferentiated oceanic arcs. Continental margins can be classified into passive and active types. Passive margin provenance is characterized by REE patterns being uniform and similar to PAAS (Bhatia 1985; McLennan 1989). Sediments deposited at active continental margins generally show a REE pattern intermediate between a "typical andesite pattern" and PAAS or in some cases indistinguishable from PAAS itself (McLennan 1989). Thus, the most active continental margin sediments display intermediate REE abundances, variable LREE enrichments and variable negative Eu anomalies, with Eu/Eu*$_{CN}$ in the range of 0.6–1.0 (McLennan 1989). Compared to the average PAAS, the Upper Triassic shale of Baluti Formation has relatively lower LREE [i.e., (La/Sm)$_{CN}$, (La/Yb)$_{CN}$ ratios] and higher Eu/Eu*$_{CN}$ ratios (Table 3), suggesting deposition in an active continental margin rather than passive margin tectonic environment (McLennan 1989; Asiedu et al. 2000)

Paleoredox conditions and trace element enrichments

Some trace elements and their ratios are considered as useful tools for determination paleoredox conditions of the clastic rocks. Some multi valence trace elements such as V, Mo, U, and Ni, their mobilization, precipitation, and concentration are mostly controlled by redox conditions and thus considered as redox-sensitive elements that are usually enriched in anoxic sediments (Dypvik 1984; Yarincik et al. 2000; Yang et al. 2004; Guo et al. 2007). The elemental ratios such as U/Th, V/Cr, V/Sc, and Cu/Zn have been used to evaluate paleoredox
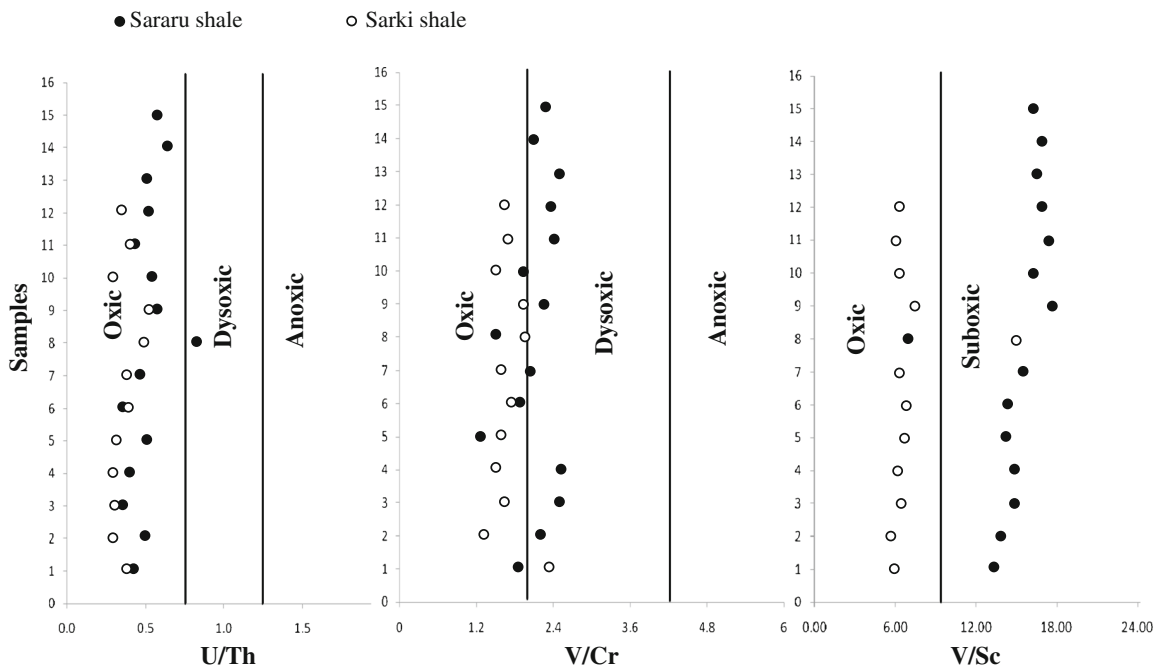
Fig. 11 Chemostratigraphic profiles of redox-sensitive trace element ratios for the Baluti Formation (the boundaries after McKirdy et al. 2011; Sari and Koca 2012)

conditions (Hallberg 1976; Jones and Manning 1994; Akinyemi et al. 2013). The ratio of U to Th may be used as a redox indicator with U/Th ratio being higher in organic rich mudstones (Jones and Manning 1994). U/Th ratios below 1.25 suggest oxic conditions of deposition, whereas values above 1.25 indicate suboxic and anoxic conditions (Jones and Manning 1994; Nath et al. 1997). The present study shows low U/Th ratio (0.48 and 0.36 in Sararu and Sarki, respectively); this indicates that these shale samples were deposited in an oxic environment. Numbers of authors have used V/Cr ratio as an index of paleo-oxygenation (Dill 1986; Dill et al. 1988; Nagarajan et al. 2007; Akinyemi et al. 2013). Bjorlykke (1974) reported the incorporation of Cr in the detrital fraction of sediments and its possible substitution for Al in the clay structure. Vanadium may be bound to organic matter by the incorporation of V^{4+} into porphyrins, and is generally found in sediments deposited in reducing environments (Shaw et al. 1990). According to Jones and Manning (1994), the V/Cr ratios above 2 indicate anoxic conditions, whereas values below 2 suggest more oxidizing conditions. In the present study, the V/Cr ratios of the Sararu shale vary between 1.26 and 2.54 with average = 2.09, and from 1.30 to 2.33 with average = 1.71 from Sarki. This indicates that they were deposited in an oxic depositional environment with an indication that some of the Sararu shale is deposited under less oxygen. V/Sc was also used to differentiate the redox condition; the samples of Sararu fall in the suboxic and for the Sarki within the oxic fields (Fig. 11). The Cu/Zn ratio is also used as a redox parameter (Hallberg 1976). According to Hallberg (1976), high Cu/Zn ratios indicate reducing depositional conditions, while low Cu/Zn ratios suggest oxidizing conditions. Therefore, the low Cu/Zn ratios in the studied shale samples (Table 2) indicate that they were deposited under oxidizing conditions. Accordingly, the oxic conditions are most predominant for the deposition of the Baluti and Sarki shales deposited under more oxic environment than Sararu shale.

Conclusions

The clay minerals of the Baluti shale comprise kaolinite, illite, and mixed layers illite/smectite at the Sararu section; and illite > smectite with traces of kaolinite at Sarki. Calcite and minor amount of quartz are the main non clay fractions in Sararu; and dolomite with subordinate amounts of calcite and quartz in Sarki. The shale of the Baluti Formation shows high CaO content (due to the high carbonate content), which have a dilution effect on the other major oxides and trace and rare earth elements. The mineralogical and geochemical parameters like illite crystallinity, CIA values, and A–CN–K diagram reveal moderate to intense chemical weathering in the source area. Major, trace, and rare earth elements imply that the shales of Baluti Formation was derived from dominantly felsic-

intermediate source rocks with the effect of mafic rocks on the Sararu shale. The probable source of the sediments is from the plutonic-metamorphic complex of the Arabian Shield and Rutba Uplift to the southwest of the basin, whereas the Sararu shale is affected by the mafic rocks from the Bitlis-Avroman-Bisitoun Ridge to the north and northeast of the basin. The tectonic setting discrimination diagram reveals active continental margin tectonic environment for the source area, and the part of sediments of Sararu are derived from more passive environment. The U/Th, V/Cr, V/Sc, and Cu/Zn ratios and negative Eu anomaly (Eu/Eu*$_{CN}$) suggest the deposition under an oxic environment and more oxic for Sarki shale.

References

Absar N, Sreenivas B (2015) Petrology and geochemistry of greywackes of the ~1.6 Ga middle Aravalli Supergroup, Northwest India: evidence for active margin processes. Int Geol Rev 57:134–158

Akinyemi SA, Adebayo OF, Ojo OA, Fadipe OA, Gitari WM (2013) Mineralogy and geochemical appraisal of paleo-redox indicators in Maastrichtian outcrop shales of Mamu formation, Anambra Basin, Nigeria. J Natur Sci Res 3:48–64

Armstrong-Altrin JS (2015) Evaluation of two multidimensional discrimination diagrams from beach and deep-sea sediments from the Gulf of Mexico and their application to Precambrian clastic sedimentary rocks. Int Geol Rev 57(11–12):1446–1461

Armstrong-Altrin JS, Verma SP (2005) Critical evaluation of six tectonic setting discrimination diagrams using geochemical data of neogene sediments from known tectonic setting. Sed Geol 177:115–129

Armstrong-Altrin JS, Lee YI, Kasper-Zubillaga JJ, Carranza-Edwards A, Garcia D, Eby N, Balaram V, Cruz-Ortiz NL (2012) Geochemistry of beach sands along the western Gulf of Mexico, Mexico: implication for provenance. Chem Erde Geochem 72:345–362

Armstrong-Altrin JS, Lee YI, Verma SP, Ramasamy S (2004) Geochemistry of sandstones from the upper Miocene Kudankulam formation, southern India: implications for provenance, weathering, and tectonic setting. J Sed Res 74(2):285–297

Armstrong-Altrin JS, Nagarajan R, Lee YI, Kasper-Zubillaga JJ, Córdoba-Saldaña LP (2014) Geochemistry of sands along the San Nicolás and San Carlos beaches, gulf of California, Mexico: implication for provenance. Turk J Earth Sci 23:533–558

Asiedu DK, Suzukis SI, Nogami K, Shibata T (2000) Geochemistry of lower Cretaceous sediments, inner zone of Southwest Japan: constraints on provenance and tectonic environment. Geochem Jour 34:155–173

Avigad D, Sandler A, Kolodner K, Stern RJ, McWilliams M, Miller N, Beyth M (2005) Mass-production of Cambro-Ordovician quartz-rich sandstone as a consequence of chemical weathering of pan-African terranes: environmental implications. Earth and Planet Sci Letters 240:818–826

Bellen RC, Dunnington HV, Wetzel R, Morton D (1959) Lexique Stratigraphique Internal Asie. Iraq. International Geological Congress. Comm. Stratigr. 3, Fasc. 10a, 333p.

Bhatia MR (1983) Plate tectonics and geochemical composition of sandstones. J Geol 91:611–627

Bhatia MR (1985) Rare earth element geochemistry of Australian Paleozoic graywackes and mud rocks: provenance and tectonic control. Sed Geo 45:97–113

Bhatia MR, Crook KAW (1986) Trace element characteristics of greywackes and tectonic setting discrimination of sedimentary basins. Contrib Mineral Petrol 92:181–193

Bjorlykke K (1974) Geochemical and mineralogical influence of Ordovician island arcs on epicontinental clastic sedimentation: a study of lower Palaeozoic sedimentation in the Oslo region, Norway. Sedimentology 21(2):251–272

Bolton CMG (1958) The geology of Ranya. Manuscript report no.271. GEOSURV, Baghdad

Buday T (1980) The regional geology of Iraq, stratigraphy and paleontology. University of Mosul, Dar Al-Kutb Publishing House, Mosul

Cao J, Wu M, Chen Y, Hu K, Bian L, Wang L, Zhang Y (2012) Trace and rare earth element geochemistry of Jurassic mudstones in the northern Qaidam Basin, Northwest China. Chem Erde 72:245–252

Carroll D (1970). Clay minerals: a guide to their x-ray identification. Geol Soc Am, 80p

Chamley H (1989) Clay sedimentology. Springer Verlag, Berlin and New York

Condie KC (1993) Chemical composition and evolution of the upper continental crust: contrasting results from surface samples and shales. Chem Geol 104:1–37

Condie KC, Wronkiewicz DJ (1990) The Cr/Th ratio in Precambrian pelites from the Kaapvaal craton as an index of craton evolution. Earth and Planet Sci Letters 97:256–267

Condie KC, Boryta MD, Liu J, Quian X (1992) The origin of khondalites: geochemical evidence from the Archean to early Proterozoic granulitic belt in the North China craton. Precam Research 59(3–4):207–223

Cox R, Lowe DR, Cullers RL (1995) The influence of sediment recycling and basement composition on evolution of mudrock chemistry in the southwestern United States. Geochim Cosmochim Acta 59(14): 2919–2940

Cullers RL (1994) The controls on major and trace element variation of shales, siltstones, and sandstones of Pennsylvanian-Permian age from uplifted continental blocks in Colorado to platform sediment in Kansas, USA. Geochim Cosmochim Acta 58:4955–4972

Cullers RL (1995) The controls on the major and trace element evolution of shales, siltstones and sandstones of Ordovician to tertiary age in the Wet Mountain region, Colorado, U.S.A. Chem Geol 123(1–4): 107–131

Cullers RL, Podkovyrov VN (2000) Geochemistry of the Mesoproterozoic Lakhanda shales in southeastern Yakutia, Russia: implications for mineralogical and provenance control, and recycling. Precambrian Res 104:77–93

Cullers RL, Chaudhuri S, Kilbane N, Koch R (1979) Rare earths in size fractions and sedimentary rocks of Pennsylvanian-Permian age from the mid-continent of the USA. Geochim Cosmochim Acta 43:1285–1302

Cullers RL, Basu A, Suttner L (1988) Geochemical signature of provenance in sand-size material in soils and stream sediments near the Tobacco Root batholith, Montana, USA. Chem Geol 70(4):335–348

Dabard MP (1990) Lower Brioverian formations (upper Proterozoic) of the Armorican massif (France): geodynamic evolution of source areas revealed by sandstone petrography and geochemistry. Sed Geol 69:45–58

Dai S, Graham IT, Ward CR (2016) A review of anomalous rare earth elements and yttrium in coal. Int J Coal Geol 159:82–95

Dai S, Liu J, Ward CR, Hower JC, French D, Jia S, Hood MM, Garrison TM (2015) Mineralogical and geochemical compositions of late

Permian coals and host rocks from the Guxu coalfield, Sichuan Province, China, with emphasis on enrichment of rare metals. Int J Coal Geol. doi:10.1016/j.coal. 2016.04.005

Dickinson WR, Suczek CA (1979) Plate tectonics and sandstone compositions. Amer Assoc Petrol Geol Bull 63:2164–2182

Dill IH (1986) Metallogenesis of early Paleozoic graptolite shales from the Graefenthal Horst (northern Bavaria-Federal Republic of Germany). Econ Geol 81:889–903

Dill H, Teshner M, Wehner H (1988) Petrography, inorganic and organic geochemistry of lower Permian carboniferous fan sequences (Brandschiefer series) FRG: constraints to their palaeogeography and assessment of their source rock potential. Chem Geol 67(3–4):307–325

Dokuzi A, Tanyolu E (2006) Geochemical constraints on the provenance, mineral sorting and subaerial weathering of lower Jurassic and upper cretaceous clastic rocks of the Eastern Pontides, Yusufeli (Artvin), NE Turkey. Turk J Earth Sci 15:181–209

Dypvik H (1984) Geochemical compositions and depositional conditions of upper Jurassic and lower cretaceous Yorkshire clays, England. Geol Magaz 121(5):489–504

Fedo CM, Nesbitt HW, Young GM (1995) Unraveling the effects of potassium metasomatism in sedimentary rocks and paleosols, with implications for paleoweathering conditions and provenance. Geology 23:921–924

Floyd PA, Leveridge BE (1987) Tectonic environment of the Devonian Gramscatho basin, South Cornwall: framework mode and geochemical evidence from turbiditic sandstones. J Geol Soci London 144: 531–542

Friedman G, Johnson KG (1982) Exercises in sedimentology. John Wiley and Sons, New York

Garcia D, Fonteilles M, Moutte J (1994) Sedimentary fractionations between Al, Ti, and Zr and the genesis of strongly peraluminous granites. J Geol 102:411–322

Garver JI, Scott TJ (1995) Trace elements in shale as indicators of crustal provenance and terrane accretion in the southern Canadian cordillera. Geol Soci Amer Bull 107:440–453

Ghandour IM, Masuda H, Maejima W (2003) Mineralogical and chemical characteristics of Bajocian-Bathonian shales, G. Al-Maghara, North Sinai, Egypt: climatic and environmental significance. Geochem J 37:87–108

Girty GH, Barber RW (1993) REE, Th, and Sc evidence for the depositional setting and source rock characteristics of the Quartz Hill chert, sierra Nevada, California. Processes controlling the composition of clastic sediments (Johnsson, M. J. And Basu, a., eds.). Geol Soc Amer Spec Pap 284:109–119

Girty GH, Ridge DL, Knaack C, Johnson D, Al-Riyami RK (1996) Provenance and depositional setting of Paleozoic chert and argillite. Sierra Nevada, California J Sed Res 66:107–118

Grim RE (1968) Clay mineralogy, 2nd edn. McGraw-Hill, New York

Gu XX (1996) Geochemical characteristics of the Triassic Tethys sediments in NW-Sichuan and its implications to the weathering conditions in source regions. Miner Petro Geochem Bull 15:23–27

Gu XX, Liu JM, Zheng MH (2002) Provenance and tectonic setting of the Proterozoic turbidites in Hunan, South China: geochemical evidence. J Sed Research 72:393–407

Guo QJ, Shields GA, Liu CQ, Strauss H, Zhu MY, Pi DH, Goldberg T, Yang XL (2007) Trace element chemostratigraphy of two Ediacaran-Cambrian successions in South China: implications for organo-sedimentary metal enrichment and silicification in the early Cambrian. Paleogeog Paleoclimat Paleoecol 254:194–216

Hallam A, Grose JA, Ruffell AH (1991) Paleoclimatic significance of changes in clay mineralogy across the Jurassic-Cretaceous boundary in England and France. Palaeogeog Palaeoclimat Palaeoecol 81:173–187

Hallberg RO (1976) A geochemical method for investigation of paleoredox conditions in sediments. Ambio Special Report 4: 139–147

Hanna MT (2007) Palynology of the upper part of Baluti Formation (Upper Triassic) and the nature of its contact with the Sarki Formation (Lower Jurassic) at Amadiya district, Northern Iraq. Unpubl PhD Thesis. Mosul University. 143p

Hardy RG, Tucker ME (1988) X-ray powder diffraction of sediments. In: Tucker ME (ed) Techniques in sedimentology. Blackwell Scientific Publications, Oxford, pp 191–228

Hayashi K, Fujisawa H, Holland HD, Ohmoto H (1997) Geochemistry of ~1.9 Ga sedimentary rocks from northeastern Labrador, Canada. Geochim Cosmochim Acta 61:4115–4137

Hosseininejad S, Pedersen PK, Spencer RJ, Nicolas MPB (2012) Mineralogy, geochemistry and facies description of a potential Cretaceous shale gas play in western Manitoba (part of NTS 63 K12). In: Report of Activities 2012, Manitoba Innovation, Energy and Mines, Manitoba Geological Survey, p 151–159

Hu J, Li Q, Huang J, Ge D (2015) Geochemical characteristics and depositional environment of the middle Permian mudstones from central Qiangtang Basin, northern Tibet. Geol J doi. doi:10.1002/gj.2653

Jassim SZ, Goff JC (2006) Phanerozoic development of the Northern Arabian Plate. In: Jassim SZ, Goff JC (eds) Geology of Iraq. Dolin. Prague and Morarian Museum, Brno, pp 15–34

Jassim SZ, Buday T, Cicha I (2006) Tectonic framework. In: Jassim SZ, Goff JC (eds) Geology of Iraq. Dolin. Prague and Morarian Museum, Brno, pp 45–56

Jones B, Manning DAC (1994) Comparison of geochemical indices used for the interpretation of paleoredox conditions in ancient mudstones. Chem Geol 111:111–129

Khanehbad M, Moussavi-Harami R, Mahboubi A, Nadjafi M, Mahmudy Gharaie MH (2012) Geochemistry of carboniferous sandstones (Sardar formation), East-Central Iran: implication for provenance and tectonic setting. Acta Geol Sin 86:1200–1210

LaMaskin TA, Dorsey R, Vervoort JD (2008) Tectonic controls on mudrock geochemistry, Mesozoic rocks of eastern Oregon and western Idaho, USA: implications for cordilleran tectonics. J Sed Res 78(12):765–783

Mader D, Neubauer F (2004) Provenance of Paleozoic sandstones from the Carnic alps (Austria): petrographic and geochemical indicators. Inter J Earth Sci 93:262–281

Madhavaraju J, Ramasamy S (2002) Petrography and geochemistry of late Maastrichtian-early Paleocene sediments of Tiruchirapalli cretaceous, Tamil Nadu—paleoweathering and provenance implications. J Geol Soc India 59:133–142

Maynard JB (1992) Chemistry of modern soils as a guide to interpreting Precambrian paleosols. J Geol 100:279–289

McKirdy DM, Hall PA et al (2011) Paleoredox status and thermal alteration of the lower Cambrian (series 2) Emu Bay shale Lagerstätte, South Australia. Australian J Earth Sci 58:259–272

McLennan SM (1989) Rare earth elements in sedimentary rocks: influence of provenance and sedimentary processes. Rev Miner Geochem 21:169–200

McLennan SM, Taylor SR (1991) Sedimentary rocks and crustal evolution: tectonic setting and secular trends. J Geol 99:1–21

McLennan S, Hemming S, McDaniel D, Hanson G (1993) Geochemical approaches to sedimentation, provenance, and tectonics. Geol Soc Am Spec Pap 284:21–40

McLennan SM, Taylor SR, Kroner A (1983) Geochemical evolution of Archean shales from South Africa. The Swaziland and Pongola Supergroups. Precam Research 22(1–2):93–124

McLennan SM, Taylor SR, Mcculloch MT, Maynard JB (1990) Geochemical and Nd-Sr isotopic composition of deep-sea turbidites: crustal evolution and plate tectonic associations. Geochim Cosmochim Ac 54:2015–2050

Merriman RJ, Frey M (1999) Patterns of very low-grade metamorphism in metapelitic rocks. In: Frey M, Robinson D (eds) Low-grade metamorphism. Blackwell Science, Oxford, pp 61–107

Moghazi AM (2003) Geochemistry and petrogenesis of a high-K calc-alkaline Dokhan volcanic suite. South Safaga area, Egypt: the role of late Neoproterozoic crustal extension. Precam Research 125:116–178

Nagarajan R, Madhavaraju J, Nagendra R, Armstrong-Altrin JS, Moutte J (2007) Geochemistry of Neoproterozoic shales of the Rabanpalli formation, Bhima Basin, northern Karnataka, southern India: implications for provenance and paleoredox conditions. Revista Mexicana de Ciencias Geologicas 24:150–160

Nath BN, Bau M, Ramalingeswara Rao B, Rao CM (1997) Trace and rare earth elemental variation in Arabian Sea sediments through a transect across the oxygen minimum zone. Geochim Cosmochim Acta 61(12):2375–2388

Nesbitt HW, Young GM (1982) Early Proterozoic climates and plate motions inferred from major element chemistry of lutites. Nature 299:715–717

Nesbitt HW, Young GM (1984) Prediction of some weathering trends of plutonic and volcanic rocks based on thermodynamic and kinetic considerations. Geochim Cosmochim Acta 48:1523–1534

Nesbitt HW, Markovic G, Price RC (1980) Chemical processes affecting alkalies and alkaline earths during continental weathering. Geochim Cosmochim Acta 44:1659–1666

Numan NMS (1997) A plate tectonic scenario for the Phanerozoic succession in Iraq. Iraqi Geol J 30:1–28

Nyakairu GWA, Koeberl C (2001) Mineralogical and chemical composition and distribution of rare earth elements in clay-rich sediments from Central Uganda. Geochem J 35:13–28

Potter PE, Maynard JB, Depetris PJ (2005) Mud and mudstones: introduction and overview. Springer-Verlag, New York

Purevjav N, Roser B (2012) Geochemistry of Devonian-carboniferous clastic sediments of the Tsetserleg terrane, Hangay Basin, Central Mongolia: provenance, source weathering, and tectonic setting. Island Arc 21:270–287

Raucsik B, Merényi L (2000) Origin and environmental significance of clay minerals in the lower Jurassic formations of the Mecsek Mts., Hungary. Acta geol. Hungarica 43:405–429

Roser BP, Korsch RJ (1986) Determination of tectonic setting of sandstone-mudstone suites using SiO_2 content and K_2O/Na_2O ratio. J Geol 94:635–650

Ryan KM, Williams DM (2007) Testing the reliability of discrimination diagrams for determining the tectonic depositional environment of ancient sedimentary basins. Chem Geol 242:103–125

Sari A, Koca D (2012) An approach to provenance, tectonic and redox conditions of Jurassic-Cretaceous Akkuyu formation, central Taurids, Turkey. Miner Research Explor Bull 144:51–74

Shadan M, Hosseini-Barzi M (2013) Petrography and geochemistry of the Ab-e-Haji Formation in central Iran: implications for provenance and tectonic setting in the southern part of the Tabas block. Revi Mexide Cien Geol 30:80–95

Shaw TJ, Geiskes JM, Jahnke RA (1990) Early diagenesis in differing depositional environments: the response of transition metals in pore water. Geochim Cosmochim Acta 54(5):1233–1246

Sheldon ND (2003) Pedogenesis and geochemical alteration of the picture gorge subgroup, Columbia River basalt, Oregon. Geol Soc Am Bull 115:1377–1387

Shynu R, Rao P, Parthiban G, Balakrishnan S, Narvekar T, Kessarkar PM (2013) REE in suspended particulate matter and sediment of the Zuari estuary and adjacent shelf, western India: influence of mining and estuarine turbidity. Mar Geol 346:326–342

Singer A (1984) The paleoclimatic interpretation of clay minerals in sediments: a review. Earth Sci Rev 21:251–293

Sissakian VK (2000) Geological map of Iraq (scale 1:1000000, sheet no.1, 3rd edition). GEOSURV, Baghdad

Spalletti LA, Limarino CO, Pinol FC (2012) Petrology and geochemistry of carboniferous siliciclastic from the argentine frontal cordillera: a test of methods for interpreting provenance and tectonic setting. J S Am Earth Sci 36:32–54

Srivastava AK, Randive KR, Khare N (2013) Mineralogical and geochemical studies of glacial sediments from Schirmacher oasis, East Antarctica. Quarter Int 292:205–216

Stern RJ (1994) Arc assembly and continental collision in the Neoproterozoic east African Orogen: implications for consolidation of Gondwanaland. Annu Rev Earth Planet Sci 22:319–351

Surdashy AM (2012) Geological study of Permian-Triassic succession in Ora-Nazdur area and reservoir characterization. Internal report of Repsol Oil Company

Tawfik HA, Ghandour IM, Maejima W, Abdelhameed AT (2011) Petrography and geochemistry of the lower Paleozoic Araba formation, northern Eastern Desert, Egypt: implications for provenance, tectonic setting and weathering signature. J Geosci Osaka 54:1–16

Taylor SR, McLennan SH (1985) The geochemical evolution of the continental crust. Rev Geophys 33:241–265

Tobia FH, Shangola SS (2016) Mineralogy, geochemistry, and depositional environment of the Beduh shale (lower Triassic), Northern Thrust Zone, Iraq. Turk J Earth Sci 25:367–391

Verma SP, Armstrong-Altrin JS (2013) New multi-dimensional diagrams for tectonic discrimination of siliciclastic sediments and their application to Precambrian basins. Chem Geol 355:117–133

Weaver CE (1989) Clays, muds, shales. Developments in sedimentology. Elsevier, Amsterdam

Wronkiewicz DJ, Condie KC (1990) Geochemistry and mineralogy of sediments from the Ventersdorp and Transvaal Supergroups, South Africa: cratonic evolution during the early Proterozoic. Geochim Cosmochim Acta 54:343–354

Xiao L, Xu Y, Mei H, Zheng Y, He B, Pirajno F (2004) Distinct mantle sources of low-Ti and high-Ti basalts from the western Emeishan large igneous province, SW China: implications for plume-lithosphere interaction. Earth Planet Sci Lett 228:525–546

Yan Z, Wang Z, Yan Q, Wang T, Guo X (2012) Geochemical constraints on the provenance and depositional setting of the Devonian Liuling group, east Qinling mountains, Central China: implications for the tectonic evolution of the Qinling Orogenic Belt. J Sed Research 82:9–24

Yan Y, Xia B, Lin CX, Hu XQ, Yan P, Zhang F (2007) Geochemistry of the sedimentary rocks from the Nanxiong Basin, South China and implications for provenance, paleoenvironment and paleoclimate at the K/T boundary. Sed Geol 197:127–140

Yang JH, Jiang SY, Ling HF, Feng HZ, Chen YQ, Chen JH (2004) Paleocean-graphic significance of redox-sensitive metals of black shales in the basal lower Cambrian Niutitang formation in Guizhou Province, South China. Progress in Natur Sci J 14:152–157

Yarincik KM, Murray RW, Lyons TW, Peterson LC, Haug GH (2000) Oxygenation history of bottom waters in the Cariaco Basin, Venezuela, over the past 578,000 years: results from redox-sensitive metals (Mo, V, Mn, and Fe). Paleoceanography 15:593–604

Zaid SM (2015) Geochemistry of sandstones from the Pliocene Gabir formation, north Marsa Alam, Red Sea, Egypt: implication for provenance, weathering and tectonic setting. J Afr Earth Sci 102:1–17

Zaid SM, Gahtani FA (2015) Provenance, diagenesis, tectonic setting and geochemistry of Hawkesbury sandstone (middle Triassic), southern Sydney Basin, Australia. Turk J Earth Sci 24:72–98

Zaid SM, Elbadry O, Ramadan F, Mohamed M (2015) Petrography and geochemistry of Pharaonic sandstone monuments in tall san Al Hagr, Al Sharqiya governorate, Egypt: implications for provenance and tectonic setting. Turk J Earth Sci 24:344–364

Zhang Y, Wang Y, Geng H, Zhang Y, Fan W, Zhong H (2013) Early Neoproterozoic (~850 Ma) back-arc basin in the central Jiangnan Orogen (eastern South China): geochronological and petrogenetic constraints from metabasalts. Precam Research 231:325–342

Zimmermann U, Spalletti LA (2009) Provenance of the lower Paleozoic Balcarce formation (Tandilia system, Buenos Aires Province, Argentina): implications for paleogeographic reconstructions of SW Gondwana. Sed Geol 219(1–4):7–23